ChemComm

Cite this: *Chem. Commun.*, 2011, **47**, 9275–9292

www.rsc.org/chemcomm

FEATURE ARTICLE

Effect of size of catalytically active phases in the dehydrogenation of alcohols and the challenging selective oxidation of hydrocarbons

Qinghong Zhang, Weiping Deng and Ye Wang*

Received 26th March 2011, Accepted 5th May 2011
DOI: 10.1039/c1cc11723h

The size of the active phase is one of the most important factors in determining the catalytic behaviour of a heterogeneous catalyst. This *Feature Article* focuses on the size effects in two types of reactions, *i.e.*, the metal nanoparticle-catalysed dehydrogenation of alcohols and the metal oxide nanocluster-catalysed selective oxidation of hydrocarbons (including the selective oxidation of methane and ethane and the epoxidation of propylene). For Pd or Au nanoparticle-catalysed oxidative or non-oxidative dehydrogenation of alcohols, the size of metal nanoparticles mainly controls the catalytic activity by affecting the activation of reactants (either alcohol or O_2). The size of oxidic molybdenum species loaded on SBA-15 determines not only the activity but also the selectivity of oxygenates in the selective oxidation of ethane; highly dispersed molybdenum species are suitable for acetaldehyde formation, while molybdenum oxide nanoparticles exhibit higher formaldehyde selectivity. Cu^{II} and Fe^{III} isolated on mesoporous silica are highly efficient for the selective oxidation of methane to formaldehyde, while the corresponding oxide clusters mainly catalyse the complete oxidation of methane. The lattice oxygen in iron or copper oxide clusters is responsible for the complete oxidation, while the isolated Cu^{I} or Fe^{II} generated during the reaction can activate molecular oxygen forming active oxygen species for the selective oxidation of methane. Highly dispersed Cu^{I} and Fe^{II} species also function for the epoxidation of propylene by O_2 and N_2O, respectively. Alkali metal ions work as promoters for the epoxidation of propylene by enhancing the dispersion of copper or iron species and weakening the acidity.

State Key Laboratory of Physical Chemistry of Solid Surfaces, National Engineering Laboratory for Green Chemical Productions of Alcohols, Ethers and Esters, Department of Chemistry, College of Chemistry and Chemical Engineering, Xiamen University, Xiamen 361005, P.R. China. E-mail: wangye@xmu.edu.cn; Fax: +86-592-2183047; Tel: +86-592-2186156

1. Introduction

The function of a heterogeneous catalyst is determined by the complicated interplay of many factors. The size of the active phase is a crucial factor in controlling the catalytic performance in many systems.[1–8] It is expected that, the size of the active

Qinghong Zhang

Qinghong Zhang received her BS and MSc degrees from Nanjing University of China in 1989 and 1992, and obtained her PhD degree from Hiroshima University of Japan in 2002. She joined Xiamen University as an Associate Professor in October of 2002, and was promoted to a full Professor of Xiamen University in 2010. Her research interests include the synthesis and characterizations of novel nano-structured materials with advanced catalytic properties.

Weiping Deng

Weiping Deng received his BS degree in chemistry from Hubei University of China in 2003, and obtained his PhD degree from Xiamen University in 2009 under the guidance of Professor Ye Wang. He is currently an engineer in the National Engineering Laboratory for Green Chemical Productions of Alcohols, Ethers and Esters. He focuses on the biomass transformation catalysis and the selective oxidation catalysis.

phase may affect the coordination structure and the electronic structure of the active site, and thus may influence the activation of reactant molecules and the active species, leading to differences in activity and/or selectivity. The catalytic performance may also be altered by the tuned redox and acid–base properties owing to the change in the size of active phases. The deep understanding of the size effect in various kinds of reactions would be helpful for the rational design of highly efficient catalysts.

The active site or active centre for homogeneous and metalloenzymatic catalysis is usually quite clear and is composed of one single metal atom or a cluster of several metal atoms. For examples, a homogeneous Ti catalyst for olefin polymerization, which contains just one Ti centre coordinated by organic ligands, is usually viewed as a single-site catalyst.[9] The active centres for the selective oxidation of methane to methanol by oxygen in the soluble and particulate methane monooxygenases (sMMO and pMMO) are the binuclear iron and the binuclear or trinuclear copper centres, respectively.[10–12]

For heterogeneous catalysis, the concept of the active site was originally proposed by Taylor, who believed that only some peculiar kinds of atoms on a catalyst surface functioned in chemisorptions and catalytic reactions.[13] There exist some heterogeneous catalysts possessing structurally well-defined active sites. For examples, titanosilicate-1 (TS-1), which can catalyse various kinds of selective oxidation reactions by using hydrogen peroxide as an oxidant, functions with Ti^{IV} isolated in the framework of MFI zeolite as the active site (Fig. 1A).[14] TS-1 is known as a "single-site" heterogeneous catalyst.[14,15] Other catalysts, which contain catalytically active centres spatially isolated from each other, can also be viewed as "single-site" heterogeneous catalysts. Thomas *et al.*[15,16] divided these "single-site" heterogeneous catalysts into the following four principal categories: (i) isolated ions, atoms, molecular complexes, and bimetallic clusters anchored to oxide supports with high surface areas; (ii) immobilized asymmetric organometallic species at mesoporous solids; (iii) "ship-in-bottle" structures, in which isolated catalytic molecular entities are entrapped within zeolite cages; (iv) molecular sieves containing isolated active sites, which are uniformly distributed spatially throughout the bulk.

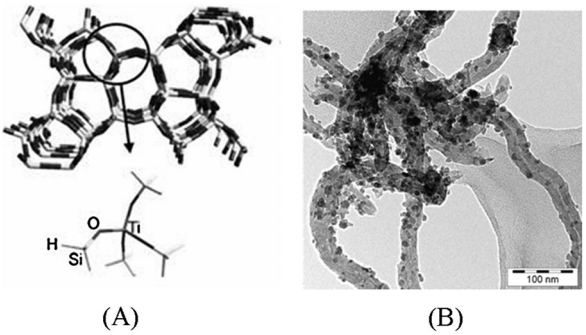

Fig. 1 Examples of active sites or active phases in heterogeneous catalytic reactions. (A) Active site of TS-1 [Reproduced with permission from Elsevier].[14] (B) TEM image of a Co/CNF catalyst efficient for FT synthesis [Reproduced with permission from American Chemical Society].[18]

However, in many cases, the structure of active sites may not be fully understood because of the complexity of solid catalysts. Usually, instead of "active site", the concept of "active phase" is used. There are many examples showing that nano-sized particles (nanoparticles) or clusters (including nano- and subnano-clusters, which typically contain several to several hundreds of atoms) are the catalytically active phase for a variety of reactions. For examples, for CO oxidation over TiO_2-supported Au catalyst, the active phase is the Au nanoparticle with sizes less than 3–5 nm;[17] the cobalt nanoparticles of ≥ 6 nm in size supported on carbon nanofibers (CNFs) (Fig. 1B) are the active phase for Fischer–Tropsch synthesis for the production of C_5^+ hydrocarbons from synthesis gas.[18]

Significant size effects have been observed in many heterogeneous catalytic systems. Such effects are prominent for Au catalysis, and have caused the "gold rush" in the past decade.[19] It now becomes clear that the size of Au nanoparticles is a predominant factor controlling their catalysis. Actually, the size effect has been studied intensively for transition metal nanoparticle-catalysed reactions, particularly hydrogenation reactions. A very important concept, *i.e.*, the structure sensitivity, was proposed by Boudart several decades ago.[20] According to this concept, if the rate per surface metal atom, *i.e.*, the turnover frequency (TOF), does not change with the size of metal particles, the reaction is defined as a structure-insensitive reaction (Fig. 2, curve III); otherwise, the reaction is a structure-sensitive reaction. There are two types of structure-sensitive reactions.[7] The TOF of Type-I reaction increases with the size of metal particles (Fig. 2, curve I), while that of Type-II reaction decreases with increasing the size of metal particles (Fig. 2, curve II). As summarized in a recent review,[7] the rate-determining step of Type-I reactions typically involves the cleavage or formation of a π-bond (*e.g.*, N_2, CO and C_2H_4 activation). The rate may show a maximum (Fig. 2, curve Ib) or may increase monotonically (Fig. 2, curve Ia) with increasing particle size. The Fe-catalysed ammonia synthesis shows Type-I behaviour, where TOF increases with the size of Fe nanoparticles from 2–12 nm.[21] Another example for Type-I behaviour is Fischer–Tropsch synthesis over CNF-supported Co nanoparticles or carbon nanotube (CNT)-supported

Ye Wang

Ye Wang received his BS and MSc degrees from Nanjing University of China, and obtained his PhD degree in 1996 from Tokyo Institute of Technology of Japan. He worked as a research associate at Tokyo Institute of Technology in 1996–1997 and Tohoku University in 1997–2000. He moved to Hiroshima University in 2000 and was promoted to Associate Professor in 2001. He became a full Professor of Xiamen University in August of 2001. He is currently the Vice Chairman of Catalysis Society of China. His main research interests are heterogeneous catalysis for selective oxidation and for energy-related processes.

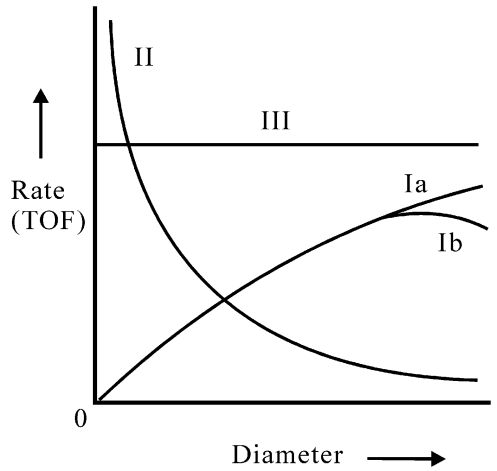

Fig. 2 Three types of structure sensitivity observed for transition metal nanoparticle-catalysed reactions [Reproduced with permission from American Chemical Society].[7] Examples: Type-I: Fe-catalysed NH_3 synthesis and Co or Ru-catalysed FT synthesis;[18,21,22] Type-II: Pt-catalysed ethane hydrogenolysis or methane reforming with CO_2 or H_2O;[21,24] Type-III: Pt-catalysed ethylene or cyclohexene hydrogenation.[21]

Ru nanoparticles.[18,22,23] Type-II reactions typically involve the activation of a σ bond (*e.g.*, C–H or C–C bond), *e.g.*, ethane hydrogenolysis and methane reforming with CO_2 or H_2O over supported Pt nanoparticles,[21,24] which requires highly reactive coordinatively unsaturated sites. The Type-III behaviour is typical for transition metal-catalysed olefin hydrogenation reactions, *e.g.*, ethylene or cyclohexene hydrogenation over supported Pt catalysts.[21]

On the other hand, studies on the size effect in oxidation reactions are not so numerous. The Au-catalysed oxidation of CO is probably the most extensively investigated oxidation reaction showing significant size effect. Several research groups elucidated that the Au nanoparticles less than 3–5 nm in diameter were catalytically active for CO oxidation.[17,25,26] Hutchings and co-workers[27] recently demonstrated that the Au clusters with a size of ~0.5 nm (containing ~10 atoms) loaded on FeO_x by a co-precipitation method were the true active phase for CO oxidation. This size was proposed to correspond to a bilayered Au structure, which was demonstrated to be more active than the monolayer structure in a model catalyst study.[26b] A subsequent study showed that the Au/FeO_x catalyst prepared by a colloidal deposition, which contained Au nanoparticles with sizes of (2.1 ± 0.54) nm, was also very active for CO oxidation, and it was argued that Au clusters of ~0.5 nm were not mandatory to achieve the high activity.[28] The effect of Au nanocluster size on CO oxidation is still ambiguous.

Many selective oxidation reactions are catalysed by supported metal oxide nanoparticles or clusters. There is little knowledge of size effects in these reactions. Grasselli once analysed the effect of the dispersion of lattice oxygen in crystalline composite metal oxides on their catalytic behaviours for partial oxidation of propylene to acrolein and found that a proper dispersion of lattice oxygen was needed for acrolein formation.[29] Otherwise, the complete oxidation would occur with high selectivity over the catalysts containing aggregated lattice oxygen atoms. Based on these analyses, Grasselli proposed the concept of "site isolation" for selective oxidation catalysis. Thomas and co-workers proposed the concept of "single site" for some liquid-phase selective oxidation reactions, *e.g.*, the oxidation of *n*-hexane to adipic acid catalysed by Co^{III} cations located in CoAlPO-18 molecular sieve.[15,16] Panov showed that the catalytic performance of Fe-ZSM-5 for the oxidation of benzene to phenol by N_2O was dependent on the size and the coordination structure of Fe species.[30] However, related studies on the selective oxidation of lower alkanes and the epoxidation of propylene, which are two of the most challenging reactions in catalysis, are still inadequate.

The dehydrogenation of alcohols to carbonyl compounds has attracted much attention in the past decade from the viewpoint of green chemistry, and many heterogeneous catalysts, particularly supported Pd and Au nanoparticles, have shown superior catalytic performances for the oxidative dehydrogenation of alcohols in the presence of O_2.[31–33] The dehydrogenation of alcohols involves the activation and cleavage of C–H bond (β-H cleavage), which is probably the rate-determining step. The insights into the effect of Pd or Au nanoparticle size in this kind of reaction may not only be useful for the preparation of highly efficient alcohol dehydrogenation catalysts but also be helpful for the design of catalysts applicable to other reactions involving C–H bond activation. However, only scattered studies have been reported so far on the size effect in the Pd or Au nanoparticle-catalysed alcohol dehydrogenation.

This article highlights the developments achieved in size-effect studies for the oxidative and non-oxidative dehydrogenation of alcohols, the selective oxidation of methane and ethane, and the epoxidation of propylene. The nature of the size effects in these systems will be discussed based on the knowledge of reaction mechanism.

2. Size effects in Pd-catalysed oxidative dehydrogenation of alcohols

The dehydrogenation of alcohols to carbonyl compounds is one of the most essential transformations in organic synthesis. The conventional technology for the transformation of alcohols to aldehydes or ketones is oxidation using stoichiometric quantities of inorganic oxidants (*e.g.*, permanganate and dichromate). This process is highly toxic and environmentally polluting because of the production of a large amount of waste solutions containing heavy metals. From the viewpoint of green chemistry, it is urgent to develop a heterogeneous catalytic route for the oxidative dehydrogenation of alcohols using O_2 or air as an oxidant. Undoubtedly, the development of highly efficient heterogeneous catalysts is the key to establishing such an environmentally friendly and economical process.

Supported Pd, Ru and Au catalysts have been reported to exhibit promising performances for the oxidative dehydrogenation of alcohols.[31–33] As compared to Ru and Au catalysts, Pd-based heterogeneous catalysts showed relatively higher activity.[34–48] The turnover frequency (TOF) for benzyl alcohol conversion exceeded 1000 h^{-1} for most supported Pd catalysts,[35,37,38,40,42–48] while it was typically less than 500 h^{-1} for most Ru-based catalysts.[31–33,49–53]

Homogeneous Pd complexes can also catalyse the oxidative dehydrogenation of alcohols. Analyses of various homogeneous

catalytic systems suggest that Pd^{II} is the active site for the dehydrogenation of alcohols to carbonyl compounds. The reduced Pd^0 must be re-oxidized to Pd^{II} by O_2, and the transformation of Pd^{II} complex into Pd^0 nanoparticles has been proposed to cause deactivation.[54] The ligands of Pd^{II} complex stable under oxidation conditions have been proposed to play an important role in minimizing the catalyst decomposition.[54] However, an induction period was observed during the oxidative dehydrogenation of 1-phenylethanol catalysed by a Pd^{II}-immobilised hydroxyapatite (HAP) catalyst, and it was clarified that the Pd^{II} species was transformed into Pd^0 nanoparticles with a mean size of 3.8 nm during the induction period.[35] A similar phenomenon was observed in the conversion of benzyl alcohol catalysed by a Pd/Al_2O_3-*ads* catalyst prepared by an adsorption method.[38] These results indicate that the Pd^0 nanoparticles are the active phase for the heterogeneous oxidative dehydrogenation of alcohols. Grunwaldt *et al.*[55] performed *in situ* XANES and EXAFS studies combined with on-line catalytic measurements using FT-IR for the oxidative dehydrogenation of benzyl alcohol over a Pd/Al_2O_3 catalyst, and the result provided further evidence that Pd^0 nanoparticles are the active phase for the dehydrogenation of alcohols, while PdO is almost inactive.

A few studies have been contributed to elucidate the size effects in the Pd particle-catalysed oxidative dehydrogenation of alcohols. Mori *et al.*[35] compared the TOFs of Pd/HAP catalysts containing Pd nanoparticles of 3.8 and 7.8 nm in size for the oxidative dehydrogenation of 1-phenylethanol and benzhydrol, and found that the catalyst with the smaller Pd particles exhibited a higher TOF in both reactions. The TOFs based on surface low-coordination Pd sites (edge and corner Pd sites) were, however, almost the same, suggesting the key role of the low-coordination Pd atoms in the oxidative dehydrogenation of alcohols.[35] The Pd/Al_2O_3-*ads* catalyst with a mean size of Pd nanoparticles of $\sim$5 nm was found to be more active than the Pd/Al_2O_3-*imp* (prepared by impregnation) containing Pd particles of $\sim$20 nm in size.[38]

Our group has performed systematic studies on the size effects in the Pd-catalysed oxidative dehydrogenation of alcohols.[43,44] One of the most important tasks is to prepare catalysts containing size-controllable Pd nanoparticles. We have succeeded in preparing two series of supported size-tuneable Pd catalysts, *i.e.*, Pd/NaX and Pd/SiO_2-Al_2O_3. The Pd/NaX catalysts were prepared by an ion exchange of Na^+ in zeolite NaX with $[Pd(NH)_4]^{2+}$ in aqueous solution, followed by calcination and reduction. The calcination temperature was found to be a crucial factor in controlling the mean size of the Pd nanoparticle.[43] The change in calcination temperature from 393 to 773 K decreased the mean size of Pd particles from 10.5 to 2.0 nm after the reduction by H_2 at 573 K (Table 1). H_2-TPR revealed that about 70–80% of Pd^{II} ions were reduced to Pd^0 nanoparticles in all these samples. The experimental fact that no reaction occurred over the unreduced catalyst suggested that only Pd^0 particles contributed to the dehydrogenation of alcohols and that the Pd^{II} ions remaining in the cation-exchanging positions were inactive. Considering that the mean size of Pd nanoparticles in each sample is larger than the size of the supercage of NaX ($\sim$1.3 nm), we believe the Pd nanoparticles are located outside of the supercage of NaX. We have analyzed the reason for why the size of Pd nanoparticles could be tuned by changing the temperature for calcination before reduction. It is known that the $[Pd(NH_3)_4]^{2+}$ species in the cation-exchanging positions of zeolite may undergo gradual changes to $[Pd(NH_3)_2]^{2+}(OZ)_2$ (OZ = lattice oxygen of zeolite) and then to $Pd^{2+}(OZ)_4$ with a rise in calcination temperature from 423 to 773 K.[56] This suggests that the interaction between the ionic Pd species and the anionic zeolite framework becomes stronger at higher calcination temperatures. The size of a metal particle is generally controlled by the rates of nucleation and of nuclei

Table 1 Mean sizes and dispersion of Pd nanoparticles supported on zeolite NaX and SiO_2–Al_2O_3

Catalyst	Pd loading (wt%)	Pd mean size[a] (nm)	Pd dispersion[b]	Pd dispersion[c]
Pd/NaX (393 K)[d]	1.35	10.5	0.06	0.11
Pd/NaX (473 K)[d]	1.35	5.4	0.18	0.21
Pd/NaX (523 K)[d]	1.35	2.9	0.31	0.39
Pd/NaX (573 K)[d]	1.35	2.8	0.31	0.40
Pd/NaX (673 K)[d]	1.35	2.6	0.35	0.43
Pd/NaX (773 K)[d]	1.35	2.0	0.57	0.56
Pd/SiO_2–*hexanol*[e]	0.55	5.7	n.d.[f]	0.20
Pd/SiO_2–Al_2O_3–*hexanol* (2/1)[e]	0.52	5.1	n.d.[f]	0.22
Pd/SiO_2–Al_2O_3–*hexanol* (1/1)[e]	0.30	4.2	n.d.[f]	0.27
Pd/SiO_2–Al_2O_3–*hexanol* (1/2)[e]	0.52	3.2	n.d.[f]	0.32
Pd/Al_2O_3–*hexanol*[e]	0.53	2.6	n.d.[f]	0.43
Pd/SiO_2–H_2[e]	0.55	10	0.04	0.11
Pd/SiO_2–Al_2O_3–H_2 (2/1)[e]	0.52	4.3	0.27	0.26
Pd/SiO_2–Al_2O_3–H_2 (1/1)[e]	0.30	3.6	0.34	0.31
Pd/SiO_2–Al_2O_3–H_2 (1/2)[e]	0.30	3.1	0.39	0.36
Pd/SiO_2–Al_2O_3–H_2 (1/2)[e]	0.52	3.1	0.37	0.36
Pd/SiO_2–Al_2O_3–H_2 (1/4)[e]	0.39	2.9	0.43	0.39
Pd/SiO_2–Al_2O_3–H_2 (1/4)[e]	0.56	3.0	0.48	0.37
Pd/Al_2O_3–H_2[e]	0.53	2.2	0.69	0.51

[a] Measured by TEM. [b] Measured by CO chemisorption. [c] Calculated using Pd dispersion = 1.12/diameter of Pd particle (from TEM, nm).[57] [d] The temperature in the parenthesis is that used for calcination before H_2 reduction. [e] The ratio in the parenthesis is the Si/Al ratio; hexanol and H_2 denote the reductants used for the preparation. [f] Not detectable; this was likely because the surface Pd sites were occupied by hexanol molecules, which were difficult to remove during the pre-treatment used for CO chemisorption (evacuation at 373 K).

growth. The Pd species possessing weaker interactions with the framework of zeolite may have higher mobility, and the rate of nuclei growth would be larger, leading to the formation of larger Pd particles. On the other hand, the stronger interactions would cause the formation of smaller Pd nanoparticles. In other words, we succeeded in controlling the size of Pd nanoparticles by tuning the interaction between the Pd precursor and the support.

By using the same idea, Pd/SiO_2–Al_2O_3 catalysts containing Pd nanoparticles with mean sizes ranging from 2.2 to 10 nm (Table 1) were further prepared.[44] This series of catalysts were prepared by adsorption of $PdCl_4^{2-}$ onto SiO_2–Al_2O_3, followed by calcination and reduction with either hexanol (at 428 K for 6 h) or H_2 (at 573 K for 0.5 h). Because the interaction between the Pd precursor and Al_2O_3 was much stronger than that between the Pd precursor and SiO_2, the size of Pd nanoparticles after reduction depended on the Si/Al ratio in the supports (Table 1). The support with a higher Al content resulted in the catalyst with smaller Pd nanoparticles after the reduction by either hexanol or H_2. XPS showed that the binding energy of Pd $3d_{5/2}$ shifted from ~336.3 eV to ~335.1 eV after the reduction by either reductant, confirming the reduction of Pd^{II} to Pd^0.

The dispersion of Pd, *i.e.*, the fraction of surface Pd atoms in all of the Pd atoms, which was measured by CO chemisorption, increased with decreasing the mean size of Pd nanoparticles (Table 1). By assuming a spherical particle model, the dispersion of Pd could also be estimated roughly from the size of Pd particles using the following equation: Pd dispersion = 1.12/Pd diameter (nm).[57] The values thus estimated were in good agreement with those measured from CO chemisorption.

The oxidative dehydrogenation of benzyl alcohol was used as a model reaction for studying the size effect. The selectivity of benzaldehyde was almost independent of the mean size of Pd nanoparticles and was always quite high (>92%) over the catalysts listed in Table 1. On the other hand, the conversion strongly depended on the mean size of Pd particles. For the Pd/NaX and the Pd/SiO_2–Al_2O_3 series of catalysts, both the smaller and larger Pd nanoparticles showed lower benzyl alcohol conversions, and the catalyst with a medium mean size of Pd particles showed the highest conversion. The TOF, *i.e.*, the initial turnover rate per surface Pd atom, was found to depend strongly on the mean size of Pd particles (Fig. 3). Moreover, all the data points in Fig. 3 obtained with different catalysts, including Pd/NaX, Pd/SiO_2–Al_2O_3-*hexanol* and Pd/SiO_2–Al_2O_3–H_2, could be fitted in one curve. This strongly suggests that the mean size of Pd nanoparticles is the essential factor determining the TOF, whereas other factors such as the Si/Al ratio in SiO_2–Al_2O_3, the reagent (H_2 or hexanol) used for reduction and the calcination temperature used for Pd/NaX preparation may influence the activity *via* changing the mean size of Pd nanoparticles. Fig. 3 clearly demonstrates that the Pd-catalysed oxidative dehydrogenation of benzyl alcohol is a structure-sensitive reaction; the catalysts with both larger and smaller mean sizes of Pd nanoparticles exhibit lower TOFs, and there is an optimum mean size (3.6–4.3 nm) of Pd nanoparticles.

The knowledge of the reaction mechanism is helpful for deep understanding of the phenomenon that there exists an optimum size of Pd nanoparticles for the oxidative dehydrogenation of benzyl alcohol. It is accepted that, the

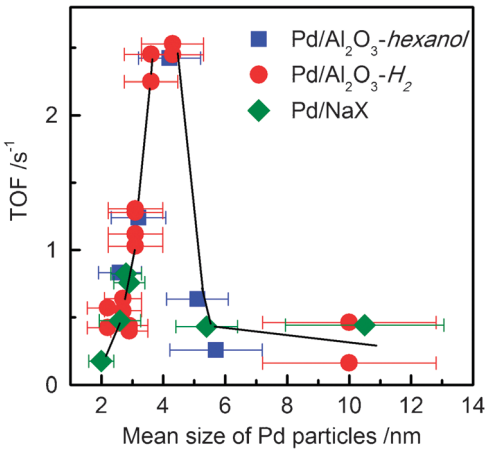

Fig. 3 Dependence of turnover frequency on the mean size of Pd nanoparticles for the oxidative dehydrogenation of benzyl alcohol. Reaction conditions: solvent-free; O_2, 3 mL min^{-1}; temperature, 343 K. The standard deviation of Pd particle size was evaluated from the particle size distribution reported previously.[43,44]

alcohol molecule is first adsorbed onto Pd surfaces, and the adsorbed alcohol undergoes activation, forming an alkoxide intermediate.[35,58–60] Then, β-H elimination occurs over the Pd surface to form aldehyde or ketone molecules. The adsorbed H species can be removed by O_2 to form H_2O. Baiker and co-workers[58–60] investigated the reaction paths for the oxidative dehydrogenation of benzyl alcohol over a Pd/Al_2O_3 catalyst using *in situ* ATR-IR spectroscopy. They proposed that the conversion of benzyl alcohol was structure insensitive, occurring indiscriminately on all Pd sites, but only selected sites may allow the desorption of benzaldehyde. This implies that the product selectivity should depend on the Pd particle size. However, the results obtained in our group showed that benzaldehyde selectivity was almost independent of the mean size of Pd nanoparticles.

On the other hand, Mori *et al.*[35] argued that the oxidative dehydrogenation of benzylic alcohols over the Pd/HAP catalyst was structure sensitive, and the coordinatively unsaturated sites (edge + corner Pd atoms) were more active than the terrace sites toward β-H elimination, which was a rate-determining step. It is known that Pd nanoparticles tend to adopt the cuboctahedral shape in the size range of 2–10 nm (Fig. 4A).[7,61,62] The fractions of terrace, edge and corner atoms on the surface of a Pd nanoparticle can be calculated using the cuboctahedral model.[61,63] The result shows that, as the particle size decreases from 10 to 2 nm, the fraction of (edge + corner) atoms increases more steeply than the fraction of terrace atoms (Fig. 4B). As a result, the ratio of the number of terrace atoms to that of (edge + corner) atoms (expressed $N_{terrace}/N_{(edge+corner)}$) declines almost linearly with decreasing the Pd particle size. Thus, if only the coordinatively unsaturated sites are crucial, TOF should increase monotonically with decreasing the mean size of Pd nanoparticles. The existence of an optimum Pd particle size may suggest that, besides the coordinatively unsaturated Pd atoms, the terrace Pd sites also play a role in the oxidative dehydrogenation of benzyl alcohol. The calculation shows that the Pd particles with sizes ranging from 3.6 to 4.3 nm, over which the highest TOF has been achieved, correspond to $N_{terrace}/N_{(edge+corner)}$ ranging from ~2.3 to

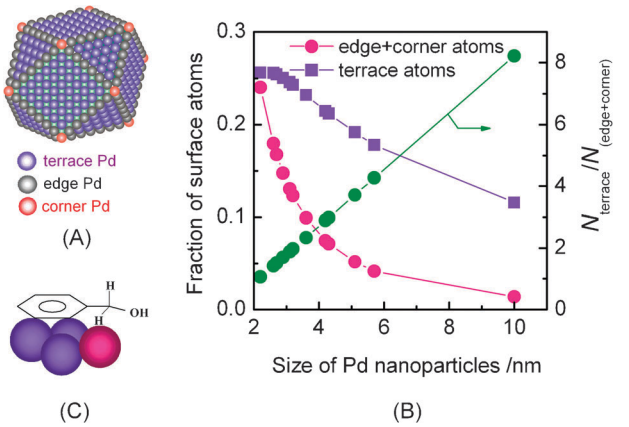

Fig. 4 (A) Cuboctahedral model for a Pd nanoparticle. (B) Dependence of fractions of surface atoms and $N_{terrace}/N_{(edge+corner)}$ on the size of Pd nanoparticles. (C) Possible adsorption model of benzyl alcohol on Pd surface.

~3.1. It is speculated that the adsorption of benzyl alcohol on Pd nanoparticles with a correct conformation (hollow site, Fig. 4C) might also be a point for its subsequent activation and conversion. The adsorption needs terrace atoms, while the β-H cleavage (C–H bond activation) requires the (edge + corner) sites. Therefore, one reasonable explanation for the optimum Pd particle size observed in Fig. 3 is that, the Pd nanoparticle with a size of ~4 nm possesses an optimum ratio of terrace to (edge + corner) Pd atoms (~3), which favours the adsorption of benzyl alcohol and the subsequent β-H cleavage. We expect that future studies using other substrates that do not contain a benzene ring may exclude the influence of substrate adsorption and may provide insights into the "intrinsic size effect" in the oxidative dehydrogenation of alcohols. Other possibilities responsible for the lower activity of the smaller Pd nanoparticles (< ~3.6 nm) may also exist. For example, stronger adsorption of O_2 over the smaller Pd nanoparticles might lead to the lower reactivity. Further clarifications are still needed in future studies.

3. Size effects in Au-catalysed oxidative or non-oxidative dehydrogenation of alcohols

Au catalysis has become a hot research area since the pioneering work of Bond, Haruta, and Hutchings.[19,64–66] Now, supported Au catalysts are known to be capable of catalyzing a variety of reactions including CO oxidation, selective oxidation, selective hydrogenation, water gas shift reaction, VOC combustion, NO_x reduction, and also many organic reactions such as C–C coupling and addition to π systems.[67] The most important feature for heterogeneous Au catalysis is the significant size effect.

Supported Au nanoparticles can efficiently catalyse the oxidative dehydrogenation of alcohols, and Au/CeO_2, Au/TiO_2, $Au/Cu_5MgAl_2O_x$, $Au/Ga_xAl_{6-x}O_9$ (x = 2, 3 and 4), Au/MnO_2, Au/hydrotalcite (HT) and Au/PCPs (PCP = porous coordination polymers) have been reported to show excellent catalytic performances.[68] However, there are only a few studies contributing to elucidating the Au size effect in the oxidative dehydrogenation of alcohols.

Tsukuda and co-workers[69,70] prepared a series of poly-(*N*-vinyl-2-pyrrolidone) (PVP)-stabilised Au nanoparticles (Au:PVP) with sizes ranging from 1.3 to 10 nm, and compared their catalytic performances in oxidative dehydrogenation of *p*-hydroxybenzyl alcohol in H_2O in the presence of K_2CO_3 promoters. They observed that, with decreasing the size of Au nanoparticles from ~10 nm, the activity appeared at an Au diameter of ~5 nm and then increased rapidly with further decreasing the size of Au clusters. Through detailed characterizations of the Au:PVP nanoclusters with different sizes by XPS, FT–IR of adsorbed CO and XANES, the catalytically active Au clusters were found to be negatively charged by electron donation from PVP.[71] PVP might play a role in regulating the electronic structure of Au nanoclusters besides function as a stabilizer. The activity was enhanced by the increased electronic density on the smaller Au nanoclusters. Based on the previous result in the gas phase that the smaller Au nanoparticles were more reactive for O_2 activation, it was proposed that the electron transfer from the anionic Au cores of Au:PVP into the LUMO (π*) of O_2 may generate superoxo- or peroxo-like oxygen species, which may be crucial for the dehydrogenation of alcohols. Tsukuda and co-workers[72] believe that the higher activity of the smaller PVP-stabilised Au nanoclusters is due to their higher O_2 activation ability. H_2O may also accelerate the activation of O_2 as demonstrated by a first-principle investigation for the coadsorption of O_2 and H_2O on small Au clusters supported on defect-free MgO(100).[73] A very recent work demonstrated that hydroxide ions played a pivotal role in the oxidative dehydrogenation of alcohols, and O_2 was proposed to participate in the reaction by regenerating the hydroxide ions *via* catalytic decomposition of a peroxide intermediate.[74]

Corma and co-workers investigated the effect of the mean size of Au nanoparticles loaded on TiO_2 on the catalytic performances for the oxidative dehydrogenation of cinnamyl alcohol.[75] They found that the TOF per surface Au atom and the product selectivity were both almost independent of the Au particle size in a range of 5–25 nm, indicating that the reaction was structure insensitive.[75] However, Baiker and co-workers reported different size effects in the supported Au-catalysed oxidative dehydrogenation of alcohols.[76,77] They prepared TiO_2- and CeO_2-supported Au catalysts with Au particle sizes ranging from 1.3 to 11 nm, and investigated their catalytic performances in the oxidative dehydrogenation of benzyl alcohol in different solvents (mesitylene, toluene and supercritical CO_2). The highest activity was obtained over the catalyst with a medium mean Au size (6.9 nm), whereas the selectivity was not significantly affected by the Au particle size and was mainly dependent on the solvent and reaction conditions.[76] The same group also compared the catalytic performances of the $Au/Cu_1Mg_2Al_1O_x$ catalysts with Au nanoparticles of ~2, ~9 and ~30 nm in size for the oxidative dehydrogenation of 1-phenylethanol, and found that the catalyst containing ~9 nm Au particles showed the highest conversion.[77] However, the intrinsic TOF was not measured in these studies.

Tsukuda and co-workers[78,79] studied the catalytic behaviours of supported Au nanoparticles (or nanoclusters) with Au sizes <2 nm for the oxidative dehydrogenation of alcohols. SBA-15-supported Au nanoclusters with a size of ~0.8 nm,

prepared by using triphenylphosphine (TPP)-protected Au_{11} clusters as precursors, were found to be effective for oxidative dehydrogenation of various alcohols by H_2O_2 under microwave irradiation.[78] A comparison among Au/SBA-15 catalysts containing Au nanoclusters with diameters of 0.8, 1.5 and 1.9 nm revealed that the catalytic activity (reaction rate counting all Au atoms) increased monotonically with decreasing the Au cluster size.[79] This phenomenon was explained by supposing that the smaller Au nanoclusters were more effective for H_2O_2 activation, which might be a key step for alcohol oxidation using H_2O_2.[79]

The presence of O_2 may cause over-oxidation and explosion or flammability of organic solvents or alcohol reactants. The safety problem becomes particularly serious for the practical large-scale transformation of alcohols to carbonyl compounds.[33] Thus, the dehydrogenation of alcohols under oxidant-free (anaerobic) conditions is a fascinating route. The dehydrogenation of alcohols in the presence of a hydrogen acceptor such as alkenes or ketones could proceed over supported Pd and Cu catalysts,[80–82] but this route consumes the hydrogen acceptor and produces organic by-products, and is not atom-economical. With respect to atom economy, the dehydrogenation of alcohols under inert atmosphere to produce carbonyl compounds and H_2 is the most desirable route. Moreover, Friedrich and Schneider[83] recently pointed out that the oxidant- and acceptor-free dehydrogenation of alcohols to carbonyl compounds and H_2 could be a promising route for H_2 synthesis and storage.

Only a few catalysts are effective for the oxidant- and acceptor-free dehydrogenation of alcohols.[84–89] In a recent communication,[90] for the first time, our group demonstrated that supported Au nanoparticles could catalyse the oxidant- and acceptor-free dehydrogenation of alcohols to aldehydes or ketones and H_2. Particularly, hydrotalcite (HT)-supported Au nanoparticles exhibited good performances in the dehydrogenation of a wide scope of alcohols including benzylic alcohols with different substituents, heteroatom-containing alcohols, aliphatic cyclic and linear alcohols. Pd/HT could also catalyse the oxidant-free dehydrogenation of alcohols,[91] but Au/HT showed higher activity and selectivity. For the dehydrogenation of benzyl alcohol, both benzyl alcohol conversion and benzaldehyde selectivity approached 100% over a 0.06 wt% Au/HT at 393 K (in 6 h of reaction). Accompanying with the conversion of benzyl alcohol to benzaldehyde, H_2 was also formed, and the amount of H_2 was almost the same with that of benzaldehyde, confirming that the dehydrogenation reaction proceeded stoichiometrically over our catalyst. The Au/HT catalyst was stable and could be used repeatedly without deactivation.

There is little information about the Au-catalysed dehydrogenation reactions in the absence of an oxidant. The nature of support and the size of Au particles are expected to play key roles in determining the catalytic behaviours in Au-catalysed dehydrogenation reactions. Rigorous study of support effects requires preparation of catalysts with similar Au particle sizes. It has been clarified that the sonication-aided impregnation, the deposition-precipitation (DP) using urea as a precipitant and the DP using NaOH as a precipitant could be used for the preparation of Au nanoparticles finely dispersed on a series of supports including SiO_2, SBA-15, carbon nanotube (CNT), Al_2O_3, TiO_2, ZrO_2, La_2O_3, CeO_2, MgO, hydroxyapatite (HAP) and HT catalysts.[92] Au nanoparticles with mean sizes of $\sim$3 nm loaded on these supports were obtained by carefully choosing the preparation conditions. The Au loading amount was 0.4–0.5 wt% in each catalyst, and XPS confirmed the presence of Au^0 over these catalysts. Catalytic studies of these catalysts for the oxidant-free dehydrogenation of benzyl alcohol showed that the Au nanoparticles loaded on SiO_2, SBA-15 and CNT exhibited very low activities (conversions $<$10% at 393 K in 6 h). Medium benzyl alcohol conversions (17–55%) were obtained when TiO_2, ZrO_2, La_2O_3 or CeO_2 was employed as the support. On the other hand, Al_2O_3-, MgO-, HAP- and HT-supported Au nanoparticles showed significantly higher benzyl alcohol conversions ($>$80%) under the same reaction conditions. Benzaldehyde selectivity strongly depended on the identity of the support. Au/SiO_2 and Au/SBA-15 showed quite lower selectivity to benzaldehyde, and the main by-product was toluene. The formation of toluene with a high selectivity was also observed in the oxidant-free dehydrogenation of benzyl alcohol over an Au–Pd/TiO_2 catalyst,[93] which was very efficient for the oxidative dehydrogenation of benzyl alcohol. The disproportionation of benzyl alcohol into benzaldehdye and toluene mainly occurs over these catalysts. On the other hand, Au/HT and Au/MgO demonstrated outstanding benzaldehyde selectivity ($>$99%). It has been clarified that the acid–base property of the support plays a key role in determining the catalytic behaviours in the dehydrogenation of benzyl alcohol. The catalyst with neither acidity nor basicity (*e.g.*, Au/SiO_2 or Au/SBA-15) was almost inactive and less selective, while that with both acidity and basicity (*i.e.*, Au/HT) exhibited both high activity and excellent selectivity. The catalyst with stronger basicity but no acidity (*e.g.*, Au/MgO) afforded higher selectivity, while that with stronger acidity but lower basicity (*e.g.*, Au/Al_2O_3) provided slightly lower selectivity.

HT-supported Au nanoparticles with mean sizes ranging from 2.1 to 21 nm were successfully prepared by varying the concentration of Au precursors and the aging temperature and time used for the DP method. The catalytic studies of these catalysts for the oxidant-free dehydrogenation of benzyl alcohol showed that benzyl alcohol conversion decreased gradually with increasing Au particle size, but benzaldehyde selectivity kept always at $\sim$100% and did not change with the Au particle size (Fig. 5A). Thus, the selectivity was dependent on the nature of support but not on the size of Au particles. The TOFs were evaluated for these catalysts using the intrinsic reaction rate, which was evaluated from the plot of benzyl alcohol conversions *versus* reaction time at the initial stage, and the dispersion of Au nanoparticles measured by H_2–O_2 titration. Fig. 5B demonstrates that the oxidant-free dehydrogenation of benzyl alcohol is a structure-sensitive reaction. The TOF increases slightly with decreasing the mean size of Au nanoparticles from 12 to $\sim$4 nm. However, a further decrease in the mean Au particle size from $\sim$4 nm increases the TOF steeply; TOF increases from $\sim$0.08 to $\sim$0.23 s^{-1} by decreasing the mean Au particle size from 4 to 2.1 nm. The TOF value of $\sim$0.23 s^{-1} ($\sim$800 h^{-1}) over the Au/HT catalyst for the oxidant-free dehydrogenation of benzyl alcohol is

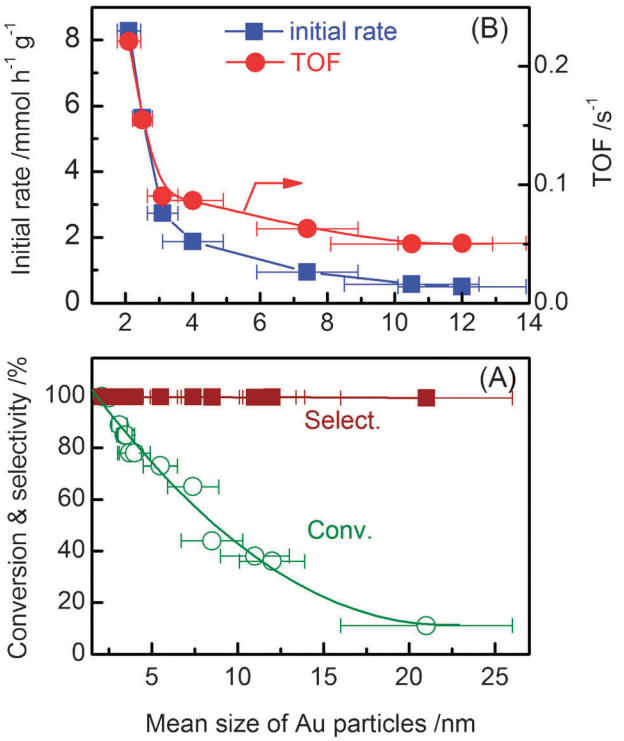

Fig. 5 Size dependence in HT-supported Au nanoparticle-catalysed oxidant-free dehydrogenation of benzyl alcohol. (A) Conversion and selectivity. (B) Initial rate and TOF for benzyl alcohol conversion. Reaction conditions: catalyst, 0.10–0.20 g (Au, 2–4 μmol); benzyl alcohol, 1–2 mmol; solvent (*p*-xylene), 5 mL; Ar flow, 3 mL min^{-1}; T = 393 K. The standard deviation of Au particle size was evaluated from particle size distribution reported previously.[92]

better than those obtained over many other catalysts such as Ag/HT (590 h^{-1}), Ag/Al_2O_3 (~10 h^{-1}), Cu/HT (<10 h^{-1}) and Pd/HT (36 h^{-1}).[87–89,91]

The observation that the TOF for oxidant-free dehydrogenation of benzyl alcohol increases steeply with decreasing the Au particle size from ~4 nm is quite different from those reported for the oxidative dehydrogenation of alcohols by the groups of Corma and Baiker,[75–77] but is similar to that reported by Tsukuda and co-workers[69–72] for the oxidative dehydrogenation of *p*-hydroxybenzyl alcohol catalysed by PVP-stabilised Au nanoclusters. Tsukuda and co-workers proposed that the smaller Au nanocluster could activate O_2 more efficiently than the larger one, and thus exhibited higher activity in the aerobic oxidation of alcohols. However, for the Au/HT-catalysed oxidant-free dehydrogenation, no oxidant has been used.

Based on mechanistic studies on Ag/Al_2O_3- and Au/HT-catalysed dehydrogenation of alcohols,[89,92] the dehydrogenation of benzyl alcohol is proposed to proceed in three main steps (Fig. 6). The first step is the activation of O–H bond of benzyl alcohol to form an alkoxide intermediate on catalyst surface. Then, the *β*-H cleavage takes place to give benzaldehyde. At the same time, a hydride species is adsorbed on the Au surface. The final step is the molecular H_2 formation from the hydride species. It is reasonable to assume that the *β*-H cleavage (C–H activation) step is the rate-determining step. The C–H bond activation or *β*-H elimination has been suggested as the rate-determining step even in the oxidative dehydrogenation

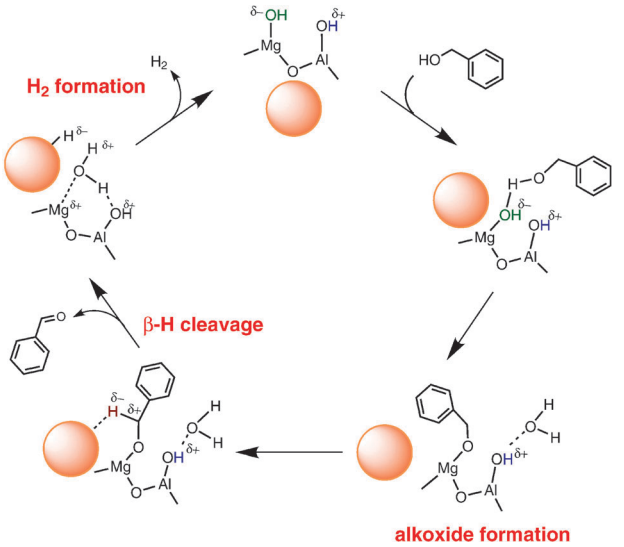

Fig. 6 Proposed reaction mechanism for the oxidant-free dehydrogenation of benzyl alcohol to benzaldehyde and H_2 over HT-supported Au nanoparticles [Reproduced with permission from Wiley].[92]

of alcohols by O_2 over several catalysts such as Ru/Al_2O_3,[49] Pd/hydroxyapatite,[35] Pd/Al_2O_3,[60] Pd/SiO_2–Al_2O_3[44] and the hydrogen-transfer dehydrogenation of alcohols catalysed by Cu/Al_2O_3.[82]

It is well known that the cleavage of *σ*-bonds including C–H bond over metal particles requires coordinative unsaturation of surface atoms (edge and corner atoms). Typically, half a truncated octahedron can be used as a model of a supported Au nanoparticle.[25,94] By using this model, the fractions of higher and lower coordination-number atoms can be estimated. The fraction of coordinatively unsaturated Au atoms increases with decreasing the size of Au particles, and such an increase becomes particularly significant as the Au particle size decreases from ~4 nm.[25,92] The variation in TOF for the dehydrogenation of benzyl alcohol with the Au particle size (Fig. 5B) corresponds well to the change in the estimated fraction of surface (corner + edge) atoms.[92] This convinces us that the coordinatively unsaturated Au sites on Au nanoparticles play a dominant role in the oxidant-free dehydrogenation of benzyl alcohol by accelerating the C–H bond activation (*β*-H cleavage).

The acid–base property of the catalyst also plays roles in the oxidant-free dehydrogenation of alcohols. A base such as K_2CO_3 often functions as an efficient promoter for the oxidative dehydrogenation of alcohols particularly in the case of Au-based catalysts.[68b,g,h,69–72,78,79] The base might function for the activation of O–H bond of alcohol to form an alkoxide intermediate.[68g] Weldon and Friend[95] pointed out that the coadsorbed oxygen atom on Au surfaces could also act as a Brønsted base, facilitating the O–H bond activation; otherwise, the activation of the O–H bond could not proceed and no alkoxide could be formed on Au surfaces. Thus, in the absence of oxidant, a base additive or basic support becomes particularly important, playing a key role in the activation of the O–H bond of alcohol, forming an adsorbed alkoxide intermediate (Fig. 6). On the other hand, the acid sites may function for the H_2 formation in the final step of Fig. 6. For the oxidative dehydrogenation of alcohols, the hydride species

is believed to be oxidized by O_2.[35,49,58–60] Under the oxidant-free conditions, the Brønsted acid sites (*i.e.*, the $AlO–H^{\delta+}$) on HT support might participate in the reaction with the Au hydride, producing molecular H_2.

4. Size effects in MoO_x-catalysed selective oxidation of ethane to oxygenates

Mo and V oxides are well-known active components in the selective oxidation of hydrocarbons. As compared to the metal nanoparticle-catalysed reactions, less knowledge is available for the size effect in the transition metal oxide-catalysed selective oxidation reactions. The size of MoO_x or VO_x species over supported catalysts was found to control their catalytic performances in the oxidative dehydrogenation of alkanes to olefins.[1,4] Oxidative dehydrogenation of lower alkanes (typically C_2H_6 and C_3H_8) are normally rate-determined by the activation of the weakest C–H bond, and the lattice oxygen is believed to play a key role.[96,97] The reaction is proposed to proceed *via* the Mars-van Krevelen mechanism, which involves the H abstraction by the lattice oxygen and the replenishment of the lattice oxygen by O_2.[98] Thus, the reactivity of the lattice oxygen species of MoO_x or VO_x particles will control the rate for the conversion of lower alkanes. Chen *et al.*[99,100] demonstrated that the rate for the oxidative dehydrogenation of C_3H_8 per Mo or V atom over the supported MoO_3 or V_2O_5 catalyst increased with increasing the size of MoO_x or VO_x clusters or particles. It was suggested that the reducibility, or the ability to accept the electrons, was enhanced over the larger MoO_x or VO_x clusters or particles owing to the lowered LUMO state.[4]

An early report showed that SiO_2-supported MoO_3 was efficient for the selective oxidation of C_2H_6 by N_2O to oxygenates (mainly acetaldehyde).[101] However, studies on MoO_x-catalysed selective oxidation of C_2H_6 to oxygenates by O_2 are limited. It is of particular interest to gain insights into how the size of MoO_x clusters or particles affect the selectivity to oxygenates.

Recently, MoO_x clusters or particles with different sizes loaded on SBA-15, a mesoporous silica material, were studied for the selective oxidation of C_2H_6 to oxygenates by O_2. It is known that, for the supported MoO_x, the position of the UV-vis absorption edge for charge-transfer transitions reflects the average size of MoO_x clusters or particles.[99,102] The edge energy values calculated from the UV-vis spectra for the MoO_x/SBA-15 catalysts with Mo contents of 2.8 and 4.9 wt% are ~4.25 eV (Fig. 7A), close to that reported for the isolated mononuclear molybdate moieties.[103] This indicates that these two catalysts are dominated by monomeric MoO_x species. The edge energy decreased significantly with increasing Mo content from 4.9 to 9.5 wt%, suggesting the aggregation of the monomeric MoO_x into oligomers or nanoclusters. With further increases in Mo content from 9.5 to 20.1 wt%, the edge energy decreased slightly. TEM measurements showed that the ordered mesoporous structure of SBA-15 was sustained for the 9.5 wt% MoO_x/SBA-15 sample. When Mo content rose to 15.4 and 20.1 wt%, collapse of the silica wall of SBA-15 occurred, and MoO_x nanoparticles of 10–20 nm in size were observed from TEM. These imply that the growth of MoO_x nanoclusters inside the mesoporous channels (channel size, ~6 nm) into MoO_x nanoparticles destroyed the amorphous silica wall of SBA-15. A drop in edge energy was observed as Mo content was raised further from 20.1 to 23.5 wt%, and needle-like MoO_3 crystallites were observed from SEM observations.

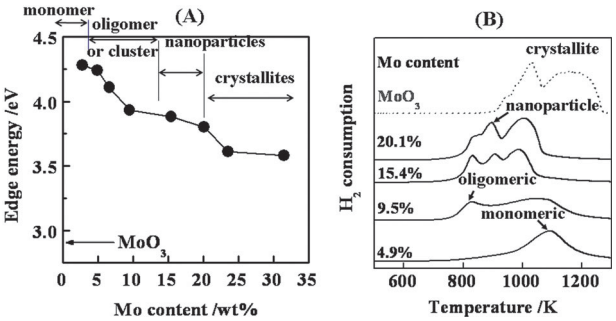

Fig. 7 (A) Dependencies of UV-vis absorption edge energy and the probable dispersion state of MoO_x species on Mo content in the MoO_x/SBA-15 catalysts. (B) H_2-TPR profiles of the MoO_x/SBA-15 catalysts with different Mo contents.

H_2-TPR profiles (Fig. 7B) also indicated the changes in MoO_x particle size with increasing Mo content.[103] For the sample with a lower Mo content (≤4.9 wt%), only a reduction peak at a higher temperature (1080–1110 K), corresponding to the reduction of the monomeric MoO_x species, was observed. The increase in Mo content to 9.5 wt% led to the appearance of a peak at ~830 K, arising from the oligomeric MoO_x species or small MoO_x nanoclusters. With a further increases in Mo content, two other peaks at 905 and 985 K, which might be ascribed to MoO_x nanoparticles, appeared.

The catalytic behaviours of the MoO_x/SBA-15 catalysts with different MoO_x particle sizes in the selective oxidation of C_2H_6 by O_2 are shown in Fig. 8. We first discuss the effect of MoO_x particle size on C_2H_6 conversion activity. C_2H_6 conversion underwent a step increase when Mo content was raised from ~6.6 wt% (Fig. 8A). The catalysts with Mo contents of 9.5–20.1 wt% exhibited remarkably higher C_2H_6 conversion rates per Mo atom than that with a lower Mo content (≤6.6 wt%).[103] Combining with the result in Fig. 7, it can be concluded that the MoO_x nanoclusters or nanoparticles are more active toward C_2H_6 activation than the monomeric MoO_x species. A similar trend was observed for the change in the rate of H_2 reduction with Mo content (Fig. 8B). Thus, the reducibility of MoO_x species is crucial in determining the rate of C_2H_6 conversion. These conclusions are in agreement with those reported by Chen *et al.*,[99] and further demonstrate that the reactivity of lattice oxygen in the MoO_x particles toward C–H cleavage depends on the particle size.

Then, we discuss the effect of MoO_x particle size on the selectivities to oxygenates. It is of significance that not only CH_3CHO but also HCHO are produced in the selective oxidation of C_2H_6 by O_2 over the MoO_x/SBA-15 catalysts.[103] The optimum Mo contents for the formations of these two kinds of oxygenates are different (Fig. 8A). The rate of CH_3CHO formation per Mo atom kept higher at Mo contents of 2.8–9.5 wt%, and an increase in Mo content to >9.5 wt% significantly decreased CH_3CHO formation rate (Fig. 8B). This indicates that the highly dispersed (monomeric and small oligomeric) MoO_x species favour the selective formation of

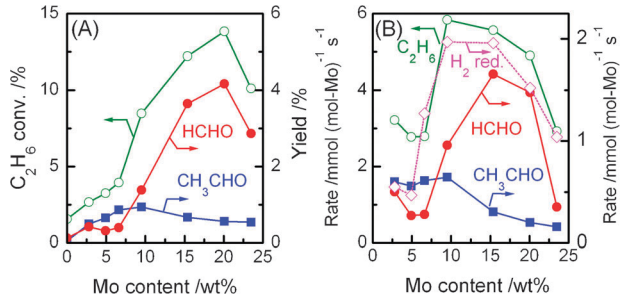

Fig. 8 Dependencies of catalytic behaviours on Mo content in the MoO_x/SBA-15 catalysts. (A) C_2H_6 conversion and product yields. (B) Rates of C_2H_6 conversion and product formation. Reaction conditions: catalyst, 0.20 g; T = 873 K; total flow rate, 150 cm^3 min^{-1}; $P(C_2H_6)$ = $P(O_2)$ = 10.1 kPa.

CH_3CHO. Grasselli[29] proposed that the high dispersion of lattice oxygen in the crystalline composite metal oxides was crucial for the selective oxidation of propylene to acrolein. Zhao *et al.*[104,105] uncovered that the high dispersion of VO_x species over SiO_2 was a key factor in the selective oxidation of C_2H_6 to oxygenates. In agreement with these, the "site isolation" is applicable to the MoO_x-catalysed selective oxidation of C_2H_6 to acetaldehyde by O_2. However, for the formation of HCHO, the situation is quite different; the presence of MoO_x nanoclusters or nanoparticles significantly accelerates the HCHO formation.

Kinetic measurements were performed to gain insights into the mechanism for CH_3CHO and HCHO formations over the MoO_x/SBA-15.[103] The results suggest that C_2H_4 and CH_3CHO are two primary products from C_2H_6, whereas HCHO is mainly formed *via* the catalytic oxidation of C_2H_4 by O_2. The investigation on the oxidation of C_2H_4 by O_2 over the MoO_x/SBA-15 catalysts with different MoO_x particle sizes reveals that higher Mo contents ($\geq$ 9.5 wt%) are required for obtaining higher HCHO selectivity (>60%) and yield (~20%), whereas CO was formed as the main product over the catalyst with a lower Mo content.[106] This suggests that MoO_x nanoclusters or nanoparticles are responsible for the selective oxidation of C_2H_4 to HCHO by O_2. The oxidation of CH_3CHO by O_2 was also performed over the MoO_x/SBA-15 catalysts, but CO was formed as a main product with a low selectivity of HCHO.[106] This excludes the possibility that HCHO is formed *via* CH_3CHO, and further confirms that HCHO is directly formed from C_2H_4 over the MoO_x/SBA-15 catalysts. Friend and co-workers[107] once investigated the C–C coupling of HCHO to form C_2H_4 on a Mo(110) surface, which is a reverse reaction of the oxidation of C_2H_4 to HCHO, and uncovered that the reaction proceeded *via* an ethylene dialkoxide intermediate. *In situ* FT–IR spectroscopic measurements for the oxidation of C_2H_4 over the MoO_x/SBA-15 catalyst also revealed an ethylene dialkoxide ($-OCH_2CH_2O-$) intermediate.[108] The conversion of C_2H_4 to HCHO is proposed to proceed with the activation of π-bond of C_2H_4, the formation of ethylene dialkoxide intermediate and the cleavage of C–C bond of the ethylene dialkoxide intermediate to form two HCHO molecules simultaneously (Fig. 9). Clearly, the monomeric MoO_x species cannot work for this mechanism, and thus, the formation of HCHO requires MoO_x nanoclusters or nanoparticles.

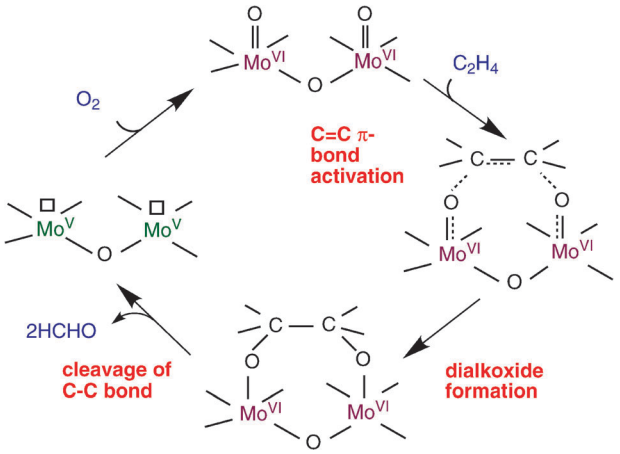

Fig. 9 Proposed reaction mechanism for the selective oxidation of ethylene by oxygen to formaldehyde over MoO_x/SBA-15 catalyst.

5. Size effects in CuO_x- and FeO_x-catalysed selective oxidation of methane to formaldehyde

The selective oxidation of methane to methanol and formaldehyde is one of the most challenging research themes in catalysis. The heterogeneous catalysts reported to date for this reaction mainly include supported metal oxides, particularly MoO_3/SiO_2 and V_2O_5/SiO_2, and composite metal oxides such as $Fe_2(MoO_4)_3$ and $FePO_4$.[108–111] Over these catalysts, HCHO single-pass yield is typically on the level of 1–2%. Two issues are believed to be responsible for the high difficulty of this reaction. First, because CH_4 is a very stable molecule, the activation of the C–H bond has to overcome a high energy barrier and usually needs stringent conditions. Second, the target products (CH_3OH or HCHO) are much more reactive than CH_4, and may easily undergo consecutive oxidations to CO and CO_2. The selectivity issue is more serious. On the other hand, methane monooxygenases (MMOs) in methanotrophic bacteria can catalyse the selective oxidation of CH_4 by O_2 efficiently under ambient conditions. In the MMOs, binuclear iron (sMMO) and bi- or tri-nuclear copper (pMMO) highly dispersed in the protein structures function as the active sites.[10–12]

The catalytic performances of various transition metal ions or oxide clusters introduced onto SBA-15 have been investigated for the selective oxidation of CH_4 by O_2.[112] The content of each transition metal (M) was kept very low (the atomic ratio of M/Si = 1/13 200) to ensure the high dispersion of these transition metal species. At such a low content, supported MoO_x and VO_x were almost inactive. On the other hand, the CuO_x on SBA-15 provided the highest HCHO formation activity; both the HCHO yield and the HCHO formation rate were the highest (Fig. 10). The FeO_x/SBA-15 and MnO_x/SBA-15 catalysts with low Fe and Mn contents also showed relatively higher HCHO formation activity. Fig. 10 suggests that the Cu, Fe and Mn sites with high dispersions are in essence highly active for HCHO formation.

Concerning the Fe-catalysed selective oxidation of CH_4 by O_2, Kobayashi *et al.*[113,114] reported that Fe^{III} highly dispersed in SiO_2 matrix was efficient for the selective formation of HCHO. Arena and Parmaliana[111] also studied the Fe-doped SiO_2 catalysts, and demonstrated that the catalyst prepared by

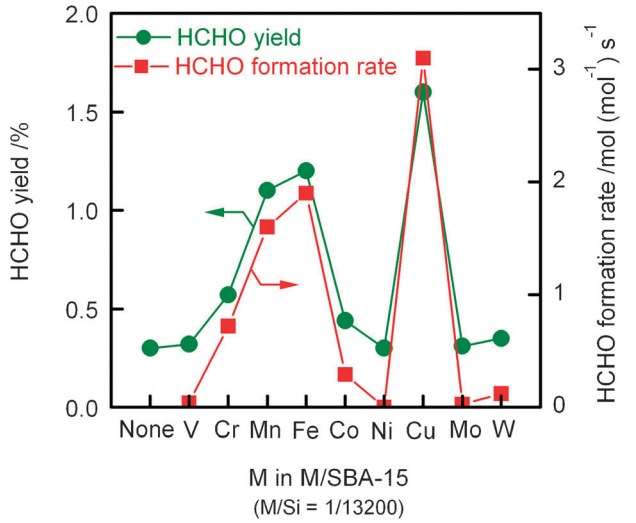

Fig. 10 Catalytic performances of various transition metal ions or oxide clusters on SBA-15 for the selective oxidation of methane by O_2. Reaction conditions: catalyst, 0.10 g; T = 898 K; total flow rate, 120 cm^3 min^{-1}; $P(C_2H_6)$ = $P(O_2)$ = 33.8 kPa.

an adsorption-precipitation method was more effective for HCHO formation than that prepared by the conventional impregnation method due to the enhanced dispersion of FeO_x species. Arena *et al.*[115] proposed that the two dimensional oligomeric FeO_x cluster possessed the best catalytic performance, while isolated FeO_x species were poor in reactivity. However, evidence has been gained in recent studies, showing that the isolated Fe^{III} site is responsible for the selective oxidation of CH_4 to HCHO. The Fe^{III} centres incorporated in the framework of SBA-15 were found to be more selective toward HCHO formation than the FeO_x clusters on the surface of SBA-15.[116] The modification of the FeO_x nanoclusters with phosphorous to form $FePO_4$ nanoclusters, in which iron sites were isolated with each other by phosphate groups, could significantly enhance HCHO selectivity at a similar CH_4 conversion level.[116] The structure-performance correlations for the selective oxidation of CH_4 over either the FeO_x/SBA-15 or the FeO_x-SiO_2 (prepared by a sol–gel method) with different Fe contents further evidence that the isolated Fe^{III} accounts for the formation of HCHO.[117,118]

There are only few reports concerning the Cu-catalysed selective oxidation of CH_4 by O_2. Groothaert *et al.*[119] demonstrated that the Cu-ZSM-5, which had been pretreated in O_2 at $\geq$ 623 K, could oxidize CH_4 to CH_3OH at $\geq$ 398 K. A charge-transfer absorption band at 22 700 cm^{-1} in the UV-vis spectrum of the pretreated Cu-ZSM-5, which may be attributable to oxygen-bridged dicopper sites, seems to correspond to the active site. A linear relationship between the intensity of this charge-transfer band and the amount of CH_3OH formed has been established.[120] Further spectroscopic characterizations combined with $^{18}O_2$ labeling experiments and DFT calculations suggested that the active species might be a bent mono-(μ-oxo)dicupric cluster located in the zeolite channel.[121] CuO_x clusters outside the zeolite channels were inactive for the oxidation of CH_4 to CH_3OH.[120] However, this reaction could not be operated in a catalytic manner, and the small amount of CH_3OH formed by the stoichiometric reaction between the active oxygen and CH_4 had to be extracted from the catalyst surface by an organic solvent such as ethanol or acetonitrile/water. Otherwise, the formed CH_3OH would undergo further oxidation to CO_2 over the Cu-ZSM-5.[119]

On the other hand, the CuO_x/SBA-15 with a very low Cu content could catalyse the selective oxidation of CH_4 to HCHO.[112] The CuO_x/SBA-15 catalysts with different copper contents were compared in the plot of HCHO selectivity *versus* CH_4 conversion, and the result showed that the catalyst with a Cu content of 0.008 wt% exhibited the highest performance for HCHO selective formation.[122] ESR investigation confirmed that this catalyst contained mainly isolated Cu^{II} sites. TOF for HCHO formation based on Cu over this catalyst reached 5.6 mol (mol–Cu)$^{-1}$ s^{-1}.[122] This value is significantly higher than those achieved over the FeO_x/SBA-15 (2.0 mol (mol–Fe)$^{-1}$ s^{-1})[117] and VO_x/SBA-15 (0.48 mmol (mol–V)$^{-1}$ s^{-1}),[123] which contained mainly isolated Fe or V sites.

CuO_x/SBA-15-*gra* catalysts prepared by a grafting method were studied for the selective oxidation of CH_4 to gain further insights into the effect of CuO_x size on catalytic performances.[124] For the preparation of CuO_x/SBA-15-*gra*, SBA-15 was first functionalized by γ-aminopropyl triethoxysilane through a reaction with hydroxyl group in dry toluene under reflux conditions. Then, copper(II) acetylacetonate was grafted onto SBA-15 by Schiff condensation between the amine group attached on SBA-15 and the carbonyl group of the acetylacetonate ligand in dry toluene.[125] Finally, the organic intermediate was calcined in air at 923 K to remove the organic groups. XRD measurements for the calcined CuO_x/SBA-15-*gra* showed that the peaks at low-diffraction angles (2θ degrees of ~1°, 1.6° and 1.9°) attributed to the hexagonal structures of mesoporous channels of SBA-15 were well sustained after the grafting of CuO_x species with contents of 0.6–2.9 wt%, and no diffraction peaks related to CuO were observed. UV-vis spectroscopic measurements showed an absorption band at ~235 nm, attributable to the charge-transfer transition between the ligand and the metal centre in isolated state, for the samples with Cu contents $\leq$1.4 wt%, and a shoulder peak at 290 nm appeared for the samples with higher Cu contents, indicating the presence of oligomeric CuO_x clusters at higher Cu contents. H_2-TPR was used to discriminate the isolated Cu^{II} sites.[126] The isolated Cu^{II} species undergoes a two-step reduction; the lower-temperature peak is ascribed to Cu^{II} to Cu^{I}, while the higher-temperature peak to Cu^{I} to Cu^{0}. On the other hand, the aggregated CuO_x clusters only show one reduction peak at lower temperatures. The fraction of isolated Cu^{II} ions evaluated from the relative intensity of the high-temperature peak decreased with increasing Cu content to >0.6 wt% for the CuO_x/SBA-15-*gra* series of catalysts, and the corresponding CuO_x/SBA-15-*imp* prepared by the impregnation method showed significantly lower fractions of Cu^{2+} (Table 2). ESR suggested that the isolated Cu^{II} was in octahedral coordination with oxygen in these samples. The intensity of ESR signal decreased because of the dipole–dipole interaction between the neighbouring Cu^{II} species as Cu content exceeded 0.6 wt%, further indicating that a part of isolated Cu^{II} began to aggregate, forming CuO_x clusters at Cu contents of >0.6 wt%.

Table 2 Catalytic performances of CuO_x/SBA-15 for the selective oxidation of CH_4 by O_2[a]

Catalyst	Fraction of isolated Cu^{2+} (%)	CH_4 conv. (%)	Selectivity[b] (%)	
			HCHO	CO_2
0.05% CuO_x/SBA-15-*gra*	~100	1.1	71	22
0.6% CuO_x/SBA-15-*gra*	96	1.8	71	18
0.5% CuO_x/SBA-15-*imp*	37	1.7	50	38
1.1% CuO_x/SBA-15-*gra*	78	1.8	65	19
1.0% CuO_x/SBA-15-*imp*	19	2.0	34	60
1.4% CuO_x/SBA-15-*gra*	50	2.2	50	30
2.9% CuO_x/SBA-15-*gra*	20	2.4	36	51

[a] Reaction conditions: W = 0.10 g, T = 898 K, $P(CH_4)$ = $P(O_2)$ = 33.8 kPa, F(total) = 120 mL min^{-1}, time on stream = 6 h. [b] The remaining product was CO.

SBA-15 itself was almost inactive for the oxidation of CH_4 under the reaction conditions in Table 2. For the CuO_x/SBA-15-*gra* series of catalysts, CH_4 conversion increased with increasing Cu content, but as Cu content exceeded 0.6 wt%, such an increase became insignificant. HCHO selectivity kept at >70% at Cu contents ≤0.6 wt%, and further increases in Cu content decreased the selectivity to HCHO, and increased that to CO_2 (Table 2). As compared with the CuO_x/SBA-15-*gra* with a similar Cu content, the CuO_x/SBA- 15-*imp* exhibited significantly lower selectivity to HCHO at a similar CH_4 conversion, while the selectivity to CO_2 was higher. These results demonstrate that the isolated Cu^{II} accounts for the selective oxidation of CH_4 to HCHO, while the CuO_x clusters are responsible for the complete oxidation of CH_4 to CO_2.

Thus, for both Cu- and Fe-catalysed selective oxidations of CH_4 by O_2, the size of the active phase plays a crucial role in controlling the product selectivity; the isolated Cu^{II} or Fe^{III} catalyses the formation of HCHO, whereas the CuO_x or FeO_x clusters mainly catalyse the formation of CO_2. Mechanistic studies by using pulse reaction technique combined with CO-adsorbed FT–IR and ESR have been performed to understand the nature of this size effect for the Cu-catalysed selective oxidation of CH_4.[122] The reaction of lattice oxygen atoms of the CuO_x/SBA-15 with CH_4 pulses at 898 K provided CO_x, suggesting that the lattice oxygen could react with CH_4, but it was not the active oxygen species for the selective formation of HCHO. On the other hand, after the pretreatment of the catalyst by CH_4 or H_2 pulses to form Cu^I, HCHO was formed during the reaction of CH_4 pulses with the O_2-pulse treated Cu^I-containing catalyst. This suggests that the activation of O_2 by Cu^I may form an active oxygen species for the selective oxidation of CH_4 to HCHO. HCHO was formed during the reactions of (CH_4 + O_2) pulses over the CuO_x/SBA-15. It is of significance that both CH_4 conversion and HCHO selectivity increase with increasing the successive pulse numbers. In other words, there is an induction period for the (CH_4 + O_2) pulse reaction. It has been clarified that the induction period depends on the ratio of CH_4/O_2; a higher CH_4/O_2 ratio leads to a shorter induction period. The presence of a small amount of H_2 in the pulse could also significantly reduce induction period. After the successive pulse reactions, a decrease in the intensity of ESR signals ascribed to Cu^{II} was observed. This indicates the reduction of Cu^{II} to Cu^I in the induction period

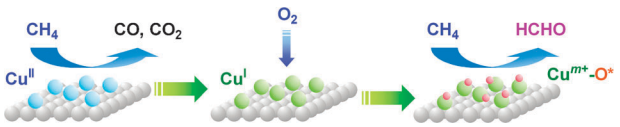

Fig. 11 Proposed reaction mechanism for the selective oxidation of methane by oxygen to formaldehyde over CuO_x/SBA-15 catalysts containing isolated Cu^{II} sites.

since Cu^I is ESR insensitive. For the 0.6 wt% CuO_x/SBA-15-*gra*, the FT–IR spectra of adsorbed CO over the fresh and the working catalysts were quite different; an intense IR band at 2131 cm^{-1} was clearly observed over the working catalyst, while the adsorption of CO over the fresh catalyst only gave an very weak IR band.[124] The former IR band is assignable to the CO adsorbed on Cu^I.[127]

All of the results described above suggest that Cu^I is generated during the reaction through the reduction of the isolated Cu^{II} site by CH_4 molecules, and the generated Cu^I functions for O_2 activation, forming an active oxygen species for the selective oxidation of CH_4 to HCHO (Fig. 11). This mechanism is quite different from the Mars-van Krevelen mechanism proposed for MoO_3/SiO_2 or V_2O_5/SiO_2 catalysts, in which the lattice oxygen is proposed for the selective oxidation of CH_4.[128,129] The lattice oxygen in the CuO_x/SBA-15 was responsible for the complete oxidation as evidenced by the pulse reaction studies. These mechanistic insights are helpful for rationalising the observed size effect. The plenty of lattice oxygen in CuO_x clusters leads to the complete oxidation, whereas the activation of O_2 on the isolated Cu^I generated from isolated Cu^{II} during the reaction can form oxygen species for selective oxidation CH_4 to HCHO.

The concept of the reductive activation of O_2 is also the case in the MMO systems.[10,11] Moreover, for the CuO_x/SBA-15 catalyst, CH_4 functions as reducing agent instead of NADH in the biological system. Concerning the nature of the active oxygen species, through DFT calculations, Yoshizawa and Shiota[130] proposed that O_2 could be activated by monomeric Cu^I species to form a Cu^{II}-superoxo (Cu^{II}–O_2^-) species. In the presence of tyrosine ligand, the Cu^{II}–O_2^- could be transformed into Cu^{II}-hydroperoxo (Cu^{II}–OOH) species *via* H-atom transfer, and the Cu^{II}–OOH could further be converted to Cu^{III}–oxo species (Cu^{III}=O) by the abstraction of an H atom from another tyrosine residue. The Cu^{III}=O could activate the C–H bond of CH_4 easily even under physiological temperatures. The activation of the C–H bond of CH_4 by the Cu^{II}–O_2^- species seems difficult under physiological temperatures because of the relatively higher energy barrier (~150 kJ mol^{-1}). However, under higher temperatures (>773 K), the Cu^{II}–O_2^- may also function for the conversion of CH_4. Actually, over the CuO_x/SBA-15 catalyst, the experimental activation energy for CH_4 conversion was ~140 kJ mol^{-1}, close to the computational energy barrier for the activation of CH_4 by the Cu^{II}–O_2^- species.

6. Size effects in CuO_x- and FeO_x-catalysed epoxidation of propylene

The epoxidation of propylene by oxygen to propylene oxide, which is a key precursor for the production of various commodity chemicals, is a highly challenging research subject

and has been regarded as the Holy Grail in catalysis.[131] Effective catalysts for the epoxidation of C_3H_6 by O_2 have not been discovered even though the Ag-catalysed epoxidation of ethylene by O_2 has been commercialized for several decades. PO selectivity is generally lower than 50% even at C_3H_6 conversions lower than 5% over most catalysts.[132]

The consecutive conversion of PO still exists as a problem. More seriously, because of the high reactivity of the allylic hydrogen atoms in C_3H_6 molecule, the allylic oxidation of C_3H_6 by the nucleophilic oxygen species may proceed quickly over most heterogeneous catalysts in the presence of O_2. Therefore, to design catalytic systems with electrophilic oxygen species is the key to increasing PO selectivity.

Much research effort has been devoted to developing new catalytic systems and catalysts capable of catalysing the selective epoxidation of C_3H_6. TS-1 catalyses the epoxidation of C_3H_6 by H_2O_2 with a high efficiency,[133] but the high cost of H_2O_2 and the use of organic solvents (such as methanol) are the main problems of this system. By using a H_2 and O_2 gas mixture, Haruta and co-workers succeeded in vapour-phase C_3H_6 epoxidation over TiO_2- or Ti-containing molecular sieve-supported Au catalyst.[134] Recently, several research groups found that the supported Au nanoparticles could catalyse the epoxidation of C_3H_6 by O_2 in the presence of H_2O.[135–137] The size of Au nanoparticles or nanoclusters is crucial for this reaction. The Au/TS-1 with a mean size of Au particles of 1.8 nm exhibited a PO selectivity of 52% at C_3H_6 conversion of 0.88% for the oxidation of C_3H_6 with O_2–H_2O at 473 K, whereas the catalyst with the same composition but a mean Au size of 4.6 nm could not catalyse the PO formation.[137] It is proposed that the reaction of O_2 and H_2O over small Au nanoclusters (<2 nm) can produce hydroperoxo (–OOH) species, which are further transferred to neighbouring Ti sites to form Ti–OOH species, and the Ti–OOH species is responsible for C_3H_6 epoxidation.[137]

For the epoxidation of C_3H_6 by O_2 alone, the supported Ag catalysts have been extensively investigated so far although the performances are far from satisfactory.[132] The size effects of Ag particles on C_3H_6 and C_2H_4 epoxidation reactions were investigated using $Ag/CaCO_3$ catalysts containing Ag particle sizes ranging from 50–600 nm.[138] The result showed that the larger Ag particles favoured C_2H_4 epoxidation by 3–5 fold, whereas particle size did not have a significant effect on C_3H_6 epoxidation. However, the selectivity to PO was very low (<10%) over the $Ag/CaCO_3$ catalysts, and the structure effect was dominated by the complete oxidation. Recently, high PO selectivity was obtained over Ag nanoparticles of ~3.5 nm in size aggregated by Ag_3 clusters deposited on ultra-thin Al_2O_3.[139]

In addition to the metallic Au and Ag nanoclusters, Cu could also catalyse the epoxidation of C_3H_6 by O_2. DFT calculations for the epoxidation of C_2H_4 over Cu(111) and Ag (111) surfaces suggested that Cu might be intrinsically more selective than Ag for the epoxidation, especially at low oxygen coverage, because the energy barrier for the conversion of oxametallocycle (OMME) intermediate to ethylene oxide was lower than that to acetaldehyde over the Cu surface, whereas the former energy barrier was higher over the Ag surface.[140] Surface science experimental studies demonstrated that *trans*-methylstyrene, a phenyl-substituted propylene, underwent efficient epoxidation on Cu(111) surfaces with oxygen adatoms despite the presence of allylic H atoms, whereas Ag(100) surface yielded only combustion products.[141] DFT calculations further indicated that the oxygen adatom on Cu(111) surface possessed lower basicity (nucleophilicity) than that on Ag(111) surface, and thus, favored the epoxidation.[142] These studies imply that Cu may be promising catalyst for the epoxidation of C_3H_6.[143] However, Monnier and Hartley[144] once pointed out that, unlike Ag, the activity of Cu(111) surface was highly dependent upon maintaining the surface as Cu^0, because Cu^0 could be easily transformed into the thermodynamically more favoured Cu^I state. The oxidic oxygen (*i.e.*, the oxygen in CuO_x) was found to be responsible for combustion of alkenes with allylic H atoms in surface science research.[141]

There exist some reports contributing to the Cu-catalysed epoxidation of C_3H_6 by O_2.[145–152] Li and co-workers showed that the pre-reduced NaCl-modified $VCe_xCu_{1-x}O_y$ and Cu/SiO_2 could catalyse the epoxidation of C_3H_6 by O_2, and proposed that Cu^0 was the active phase.[145,146] Cu/SiO_2 alone could also catalyse the epoxidation of C_3H_6 by O_2, and Cu^0 was believed to be active phase.[147] The Cu/SiO_2 prepared by a microemulsion technique containing Cu particles of ~5 nm was more selective to PO than that prepared by the conventional impregnation containing larger Cu particles. Thus, it appears that the smaller Cu^0 nanoparticles are the active phase for C_3H_6 epoxidation. However, PO formation activity was quite low over these pre-reduced Cu^0-based catalysts. Reasonably high PO selectivity (40–50%) could only be obtained at very low C_3H_6 conversions (<0.2%). PO formation rate and TOF based on Cu were lower than 0.2 mmol g^{-1} h^{-1} and 0.15 h^{-1}, respectively.

A breakthrough was made by using a halogen-free K^+-modified CuO_x/SBA-15 catalyst without pre-reduction.[148] The K^+-CuO_x/SBA-15 with copper in the oxidized state showed significantly higher PO formation activity for C_3H_6 epoxidation under O_2-rich reaction conditions.[148,149] Unlike other Cu-based catalysts probably containing Cu^0 as the active phase mentioned above, PO selectivity over this catalyst did not undergo significant decreases with increasing partial pressure of O_2 ($P(O_2)$). Thus, by increasing $P(O_2)$, C_3H_6 conversion could be raised while PO selectivity was almost kept. Under optimized conditions, the PO formation rate reached 2.1 mmol g^{-1} h^{-1}, and the TOF based on Cu was 17.5 h^{-1}, both of which were ~1 order of magnitude higher than those reported before for Cu^0-based catalysts. A K^+-modified CuO_x–SiO_2 catalyst prepared by a sol–gel method showed similar catalytic performances for the epoxidation of C_3H_6 by O_2.[150] Under O_2-rich conditions, 78% PO selectivity was obtained at 0.2% C_3H_6 conversion, and 55% PO selectivity could be sustained at a 1.4% C_3H_6 conversion.

It has been clarified that the presence of K^+ played significant roles in PO formation over the K^+-CuO_x/SBA-15 or the K^+-modified CuO_x–SiO_2 catalyst. In the absence of K^+, acrolein was the main partial oxidation product, while PO became the main partial oxidation product in the presence of K^+.[148–150] UV-vis, H_2-TPR and TEM studies for the CuO_x/SBA-15 and CuO_x–SiO_2 with and without K^+ modification showed that the presence of K^+ significantly decreased the size

of CuO_x nanoclusters or nanoparticles in these catalysts.[148–150] H_2-TPR studies suggested that this led to the decrease in the reactivity of lattice oxygen atoms in the CuO_x nanoclusters or nanoparticles. Because lattice oxygen is known to be a nucleophilic oxygen species, which is responsible for the allylic oxidation of C_3H_6 to acrolein, the decrease in the size of CuO_x nanoclusters could suppress the acrolein formation. Moreover, it was confirmed through NH_3-TPD that the presence of K^+ caused a significant decrease in the Lewis acidity of CuO_x species. Even the weak Lewis acidity is known to be capable of catalysing the isomerization of PO to allyl alcohol, which can be readily oxidized to acrolein and CO_x under oxidizing conditions.

Li and co-workers[151] confirmed that the K^+-modified CuO_x/SiO_2, which was prepared by a homogeneous deposition-precipitation method, was efficient for the epoxidation of C_3H_6 by O_2. They investigated the effect of CuO_x particle size on catalytic performances in the epoxidation of C_3H_6 by O_2. The result revealed that the smaller CuO_x nanoparticles existing in the K^+-CuO_x/SiO_2 provided better PO formation activity. When the size of CuO_x nanoparticles increased from 2.9 to 5.9 nm, PO formation rate decreased significantly from 2.5 to 0.43 mmol g^{-1} h^{-1}. It was proposed that the smaller CuO_x nanoparticles led to stronger interactions between K^+ and CuO_x species, resulting in higher PO formation activity. Recent work by Onal *et al.*[152] suggested that the isolated-like ionic Cu^{II} was responsible for the epoxidation of C_3H_6 by O_2.

FT–IR studies of adsorbed CO combined with XRD and ESR measurements were performed for the K^+–CuO_x–SiO_2 catalyst prepared by the sol–gel method under working state.[150] CO adsorbed on the fresh catalyst (after pretreatment in O_2 at 823 K) only showed a very weak IR band. After reactions in C_3H_6 and O_2 gas mixtures, a distinct IR band of adsorbed CO was observed at 2127 cm^{-1}, which was attributable to CO chemisorbed on Cu^I sites.[150] The formation of Cu^I was further confirmed by XRD for the catalyst after reaction, which revealed the formation of Cu_2O. A significant decrease in the intensity of ESR signal ascribed to Cu^{II} also indicated the partial reduction of Cu^{II} to Cu^I because Cu^I was ESR insensitive. The pre-treatment of the K^+–CuO_x–SiO_2 catalyst by H_2 reduction followed by N_2O oxidation, which could generate Cu^I with a high concentration, increased the initial PO formation rate significantly from 0.58 to 2.0 mmol g^{-1} h^{-1}. These observations all indicate that the Cu^I functions for the epoxidation of C_3H_6 by O_2 in the working catalyst. A recent study for the oxidation of C_3H_6 by O_2 over a VO_x-modified Cu catalyst, which had been pre-reduced by H_2, further excluded the possibility that Cu^0 or Cu^{II} can function for the formation of PO.[153] Therefore, it can be concluded that Cu^I is responsible for the epoxidation of C_3H_6 by O_2 over these CuO_x-based catalysts.

However, Cu_2O or supported Cu_2O is well known to catalyse the selective oxidation of C_3H_6 to acrolein by O_2.[154–157] The lattice oxygen of Cu_2O plays a key role in the formation of acrolein, and the Mars-van Krevelen mechanism seems applicable to this reaction.[157] It is of high significance that, after the modification of CuO_x nanoparticles or nanoclusters containing Cu^I by K^+, PO becomes the main partial oxidation product instead of acrolein. As described above, the size of CuO_x species is a crucial factor in the switching of the main partial oxidation product from acrolein to PO; the reactivity of lattice oxygen, which is nucleophilic in nature and is responsible for the allylic oxidation, decreases significantly owing to the decreased size of CuO_x species. It can be expected that the highly dispersed Cu^I site may activate O_2, generating electrophilic oxygen species for C_3H_6 epoxidation. Besides the decreased size of CuO_x species, K^+ also weakened the Lewis acidity of the catalyst, suppressing the consecutive conversions (*i.e.*, isomerisation and oxidation) of PO.

The FeO_x-catalysed epoxidation of C_3H_6 by N_2O represents another interesting selective oxidation system showing the size effect on product selectivity. It is known that, electrophilic oxygen species can be generated from N_2O over Fe-based catalysts, and this oxygen species can oxidize benzene and methane selectively to phenol and methanol or formaldehyde, respectively.[30,158] Duma and Hönicke first demonstrated that FeO_x supported on SiO_2 modified by Na^+ could catalyse the epoxidation of C_3H_6 by N_2O.[159] The FeO_x-catalysed C_3H_6 epoxidation by N_2O was further studied by several research groups.[160–171] An interesting phenomenon is the significant shift of reaction route from allylic oxidation to epoxidation due to modification of FeO_x nanoclusters or nanoparticles by alkali metal ions.[161,162] For example, over the 1 wt% FeO_x/SBA-15, the oxidation of C_3H_6 by N_2O produced mainly acrolein and CO_x at 598 K, and almost no PO was formed. The addition of KCl with a K/Fe molar ratio of 5 changed the main product to PO, and PO selectivity of 72% could be attained. At the same time, C_3H_6 conversion rose from 1.2% to 4.5%. The characterizations using UV-vis, XANES, EXAFS and UV-Raman suggested that, before KCl modification, the supported FeO_x catalysts (such as FeO_x/SBA-15 and FeO_x/MCM-41) mainly contained FeO_x nanoclusters, in which iron is in an octahedral coordination with oxygen, and the FeO_x nanocluster was changed into an isolated surface tetrahedral iron species after KCl modification.[162,163] The changes in the size and the coordination environment of FeO_x species owing to the alkali metal ion modification were further confirmed in a subsequent study for a Rb_2SO_4-modified FeO_x/SiO_2 by Moens *et al.*[166] It is reasonable to speculate that the FeO_x nanoclusters catalyse the allylic oxidation of C_3H_6, mainly leading to the formation of acrolein, whereas the isolated Fe^{III} in tetrahedral coordination accounts for the epoxidation of C_3H_6 by N_2O. In a word, the changes in the size and the coordination of FeO_x species mainly correspond to the change in the reaction route (Fig. 12).

H_2-TPR studies suggested that the reactivity of lattice oxygen in FeO_x nanoclusters was inhibited after the modification by KCl. Similar to the CuO_x-catalysed C_3H_6 epoxidation by O_2, the decrease in the reactivity of lattice oxygen can suppress the formation of acrolein. The increase in C_3H_6 conversions in the presence of KCl modification indicates the generation of new active oxygen species for C_3H_6 epoxidation. The isolated Fe^{II} formed during the reaction may activate N_2O, generating new electronic oxygen species for C_3H_6 epoxidation.[170] At the same time, the chloride anion may enhance the electrophilicity of the active oxygen species. The electron-deficient boron oxide was also found to be a good promoter for enhancing PO selectivity. Over B_2O_3- and K^+-doubly modified

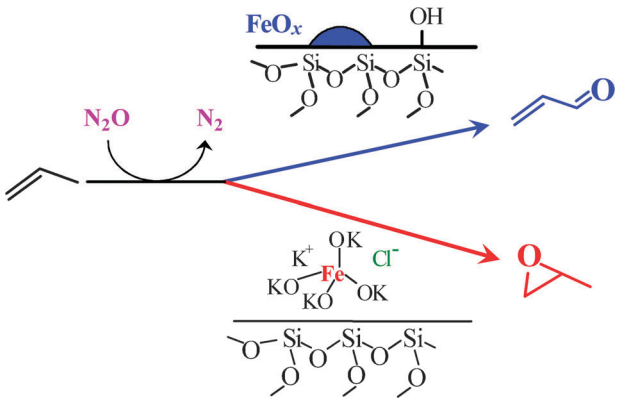

Fig. 12 Changes in the reaction route and the size of FeO_x species in the epoxidation of propylene by N_2O.

FeO_x/SBA-15 catalysts, PO selectivities of ~80 and ~70% could be attained at C_3H_6 conversions of ~5 and ~9%, respectively.[168]

7. Conclusions

Size effects in metal nanoparticle-catalysed dehydrogenation of alcohols and metal oxide nanocluster-catalysed selective oxidation of methane and ethane and epoxidation of propylene have been discussed. For the oxidative dehydrogenation of benzyl alcohol over Pd nanoparticles, the TOF reaches a maximum at a mean size of Pd particles of 3.6–4.3 nm, corresponding to the ratio of surface terrace Pd atoms to coordinatively unsaturated (edge and corner) Pd atoms being 2.3–3.1. The conformation of active sites with this ratio of different types of surface atoms may favour the adsorption of benzyl alcohol (on terrace atoms) and its subsequent β-H activation (on coordinatively unsaturated atoms). On the other hand, the reaction rate increased monotonically with decreasing the size of Au nanoparticles from 10 to 1.3 nm for the PVP-stabilized Au nanoparticles-catalysed oxidative dehydrogenation of *p*-hydroxybenzyl alcohol in water. The smaller Au nanoclusters are proposed to be more active for the activation of O_2 through the electron transfer from the negatively charged Au clusters, forming active oxygen species for alcohol conversions. Au nanoparticles supported on HT, which possesses both acidity and basicity, efficiently catalyse the oxidant- and acceptor-free dehydrogenation of alcohols to carbonyl compounds and H_2. The selectivity is mainly determined by the identity of the support, while the size of Au nanoparticles controls the activity. The TOF for benzyl alcohol conversion increases with decreasing the mean Au particle size. Particularly, TOF increases steeply when the Au particle size decreases from ~4 nm. The coordinatively unsaturated surface Au atoms are proposed to play pivotal roles in the oxidant-free dehydrogenation of alcohols. These atoms are more active for the activation of the C–H bond (β-H abstraction) in the alcohol molecules, which is believed to be the rate-determining step.

The size of the MoO_x species plays a key role in controlling the activity and selectivity for the selective oxidation of ethane by O_2. As compared to the monomeric or highly dispersed MoO_x species, the larger MoO_x nanoparticles are more active toward the conversion of C_2H_6. The reducibility of the MoO_x species is the main factor controlling C_2H_6 conversion activity. The monomeric or smaller oligomeric MoO_x nanoclusters are more selective for the formation of CH_3CHO, which is a primary product from C_2H_6, while the relatively larger MoO_x nanoparticles are suitable for the formation of HCHO. HCHO is formed *via* C_2H_4, and the selective oxidation of C_2H_4 to HCHO proceeds *via* an ethylene dialkoxide intermediate and requires the MoO_x nanoparticles.

The size of CuO_x or FeO_x species strongly affects the selectivity in the selective oxidation of CH_4 by O_2. The Cu^{II} or Fe^{III} site isolated on mesoporous silica is highly efficient for the selective oxidation of CH_4 to HCHO, while the corresponding CuO_x or FeO_x nanocluster mainly catalyses the complete oxidation of CH_4 to CO_2. That lattice oxygen atoms in CuO_x clusters are responsible for the formation of CO_2, while the isolated Cu^I generated during the reaction can activate O_2, forming active oxygen species for the selective oxidation of CH_4 to HCHO. The highly dispersed CuO_x species is also effective for the epoxidation of C_3H_6 by O_2 after the modification by alkali metal ions (*e.g.*, K^+). The modification by K^+ decreases the size of CuO_x species besides weakening the Lewis acidity. The larger CuO_x nanoclusters or nanoparticles without alkali metal ion modification provide acrolein as the main partial oxidation product. Similarly, the FeO_x nanoclusters loaded on mesoporous silica mainly catalyse the allylic oxidation of C_3H_6 to acrolein, whereas the isolated Fe^{III} in tetrahedral coordination formed by the modification of FeO_x nanoclusters with KCl or other alkali metal salts is highly selective for the formation of PO. In these two systems, the lattice oxygen atoms in the CuO_x or FeO_x nanoclusters, which are nucleophilic in nature, are responsible for the allylic oxidation to acrolein. On the other hand, the highly dispersed Cu^I or Fe^{II} sites function for the epoxidation of C_3H_6 *via* generation of electrophilic oxygen species from O_2 or N_2O.

It should be mentioned that, besides the size effect of the catalytically active phase, the support may also play important roles in determining the catalytic behaviours of supported catalysts. The typical roles of the support are to disperse the active phases or provide proper sizes of active phases and to keep the size of the active phase against sintering during the reaction. The support may also influence the chemical state of the active phase through the interaction between the active phase and the support. Furthermore, the activity or selectivity may be significantly affected by the nature of the support. The selectivity in the dehydrogenation of alcohols over supported Au or Pd nanoparticles is indeed determined by the acid–base property of the support.

The knowledge of the size effects in the dehydrogenation or selective oxidation reactions is less than that in the transition metal nanoparticle-catalysed hydrogenation reactions. This *Feature Article* demonstrates that the size of catalytically active phases (metal or metal oxide nanoparticles or nanoclusters) can not only determine the activity but also control the product selectivity. With the aid of knowledge of reaction mechanism, the size effect can provide deep insights into the true active sites working for the conversion of reactants and for the formation of different products. These insights will

undoubtedly be helpful for the rational design of highly efficient catalysts. We believe that this is particularly vital for the future breakthrough in the highly challenging selective oxidation of lower alkanes and epoxidation of propylene.

Acknowledgements

The authors gratefully acknowledge the financial support from the National Natural Science Foundation of China (Nos. 20625310, 20773099, 20873110, 20923004 and 21033006) and the National Basic Research Program of China (No. 2010CB732303).

Notes and references

1 A. T. Bell, *Science*, 2003, **299**, 1688–1691.
2 J. Grunes, J. Zhu and G. A. Somorjai, *Chem. Commun*., 2003, 2257–2260.
3 R. Schlögl and S. B. A. Hamid, *Angew. Chem., Int. Ed*., 2004, **43**, 1628–1637.
4 J. Macht and E. Iglesia, *Phys. Chem. Chem. Phys*., 2008, **10**, 5331–5343.
5 G. A. Somorjai and J. Y. Park, *Chem. Soc. Rev*., 2008, **37**, 2155–2162.
6 G. A. Somorjai and J. Y. Park, *Angew. Chem., Int. Ed*., 2008, **47**, 9212–9228.
7 R. A. van Santen, *Acc. Chem. Res*., 2009, **42**, 57–66.
8 G. A. Somorjai, H. Frei and J. Y. Park, *J. Am. Chem. Soc*., 2009, **131**, 16589–16605.
9 J. Tian, P. D. Hustad and G. W. Coates, *J. Am. Chem. Soc*., 2001, **123**, 5134–5135.
10 M. Merkx, D. A. Kopp, M. H. Sazinsky, J. L. Blazyk, J. Müller and S. J. Lippard, *Angew. Chem., Int. Ed*., 2001, **40**, 2782–2807.
11 S. I. Chan, V. C. C. Wang, J. C. H. Lai, S. S. F. Yu, P. P. Y. Chen, K. H. C. Chen, C. L. Chen and M. K. Chan, *Angew. Chem., Int. Ed*., 2007, **46**, 1992–1994.
12 R. Balasubramanian, S. M. Smith, S. Rawat, L. A. Yatsunyk, T. L. Stemmler and A. C. Rosenzweig, *Nature*, 2010, **465**, 115–119.
13 H. S. Taylor, *Proc. R. Soc. London, Ser. A*, 1925, **108**, 105–111.
14 P. Ratnasamy, D. Srinivas and H. Knözinger, *Adv. Catal*., 2004, **48**, 1–169.
15 J. M. Thomas and R. Raja, *Chem. Commun*., 2001, 675–687.
16 J. M. Thomas, R. Raja and D. W. Lewis, *Angew. Chem., Int. Ed*., 2005, **44**, 6456–6482.
17 M. Haruta, *Gold Bull*., 2004, **37**, 27–36.
18 G. L. Bezemer, J. H. Bitter, H. P. C. E. Kuipers, H. Oosterbeek, J. E. Holewijn, X. Xu, F. Kapteijn, A. J. van Dillen and K. P. de Jong, *J. Am. Chem. Soc*., 2006, **128**, 3956–3964.
19 M. Haruta, *Nature*, 2005, **437**, 1098–1099.
20 M. Boudart, *Adv. Catal*., 1969, **20**, 153–166.
21 G. A. Somorjai and J. Y. Park, *Top. Catal*., 2008, **49**, 126–135.
22 J. Kang, S. Zhang, Q. Zhang and Y. Wang, *Angew. Chem., Int. Ed*., 2009, **48**, 2565–2568.
23 Q. Zhang, J. Kang and Y. Wang, *ChemCatChem*, 2010, **2**, 1030–1058.
24 J. Wei and E. Iglesia, *J. Phys. Chem. B*, 2004, **108**, 4094–4103.
25 B. Hvolbæk, T. V. W. Janssens, B. S. Clausen, H. Falsig, C. H. Christensen and J. K. Nørskov, *Nano Today*, 2007, **2**, 14–18.
26 (*a*) Valden, X. Lai and D. W. Goodman, *Science*, 1998, **281**, 1647–1650; (*b*) M. S. Chen and D. W. Goodman, *Science*, 2004, **306**, 252–254.
27 A. A. Herzing, C. J. Kiely, A. F. Carley, P. Landon and G. J. Hutchings, *Science*, 2008, **321**, 1331–1335.
28 Y. Liu, C. J. Jia, J. Yamasaki, O. Terasaki and F. Schüth, *Angew. Chem., Int. Ed*., 2010, **49**, 5771–5775.
29 R. K. Grasselli, *Top. Catal*., 2001, **15**, 93–101.
30 G. I. Panov, *CATTECH*, 2000, **4**, 18–31.
31 T. Mallat and A. Baiker, *Chem. Rev*., 2004, **104**, 3037–3058.
32 B.-Z. Zhan and A. Thompson, *Tetrahedron*, 2004, **60**, 2917–2935.
33 T. Matsumoto, M. Ueno, N. Wang and S. Kobayashi, *Chem.–Asian J*., 2008, **3**, 196–214.
34 Y. Uozumi and R. Nakao, *Angew. Chem., Int. Ed*., 2003, **42**, 194–197.
35 K. Mori, T. Hara, T. Mizugaki, K. Ebitani and K. Kaneda, *J. Am. Chem. Soc*., 2004, **126**, 10657–10666.
36 U. R. Pillai and E. Sahle-Demessie, *Green Chem*., 2004, **6**, 161–165.
37 M. S. Kwon, N. Kim, C. M. Park, J. S. Lee, K. Y. Kang and J. Park, *Org. Lett*., 2005, **7**, 1077–1079.
38 H. Wu, Q. Zhang and Y. Wang, *Adv. Synth. Catal*., 2005, **347**, 1356–1360.
39 B. Karimi, S. Abedi, J. H. Clark and V. Budarin, *Angew. Chem., Int. Ed*., 2006, **45**, 4776–4779.
40 D. I. Enache, J. K. Edwards, P. Landon, B. Solsona-Espriu, A. F. Carley, A. A. Herzing, M. Watanabe, C. J. Kiely, D. W. Knight and G. J. Hutchings, *Science*, 2006, **311**, 362–365.
41 A. H. Lu, W. C. Li, Z. Hou and F. Schüth, *Chem. Commun*., 2007, 1038–1040.
42 C. Li, Q. Zhang, Y. Wang and H. Wan, *Catal. Lett*., 2008, **120**, 126–136.
43 F. Li, Q. Zhang and Y. Wang, *Appl. Catal., A*, 2008, **334**, 217–226.
44 J. Chen, Q. Zhang, Y. Wang and H. Wan, *Adv. Synth. Catal*., 2008, **350**, 453–464.
45 H. Wang, S. X. Deng, Z. R. Shen, J. G. Wang, D. T. Ding and T. H. Chen, *Green Chem*., 2009, **11**, 1499–1502.
46 A. Villa, D. Wang, N. Dimitratos, D. Su, V. Trevisan and L. Prati, *Catal. Today*, 2010, **150**, 8–15.
47 T. Harada, S. Ikeda, F. Hashimoto, T. Sakata, K. Ikeue, T. Torimoto and M. Matsumura, *Langmuir*, 2010, **26**, 17720–17725.
48 Y. Chen, Z. Guo, T. Chen and Y. Yang, *J. Catal*., 2010, **275**, 11–24.
49 (*a*) K. Yamaguchi and N. Mizuno, *Angew. Chem., Int. Ed*., 2002, **41**, 4538–4541; (*b*) K. Yamaguchi and N. Mizuono, *Chem.–Eur. J*., 2003, **9**, 4353–4361.
50 B. Z. Zhan, M. A. White, T. K. Sham, J. A. Pincock, R. J. Doucet, K. V. R. Rao, K. N. Robertson and T. S. Cameron, *J. Am. Chem. Soc*., 2003, **125**, 2195–2199.
51 Z. Opre, J. D. Grunwaldt, M. Maciejewski, D. Ferri, T. Mallat and A. Baiker, *J. Catal*., 2005, **230**, 406–419.
52 M. Kotani, T. Koike, K. Yamaguchi and N. Mizuno, *Green Chem*., 2006, **8**, 735–741.
53 K. Mori, S. Kanai, T. Hara, T. Muzugaki, K. Ebitani, K. Jitsukawa and K. Kaneda, *Chem. Mater*., 2007, **19**, 1249–1256.
54 S. S. Stahl, *Angew. Chem., Int. Ed*., 2004, **43**, 3400–3420.
55 J. D. Grunwaldt, M. Caravati and A. Baiker, *J. Phys. Chem. B*, 2006, **110**, 25586–25589.
56 Z. Zhang, W. M. H. Sachtler and H. Chen, *Zeolites*, 1990, **10**, 784–789.
57 N. Mahata and V. Vishwanathan, *J. Catal*., 2000, **196**, 262–270.
58 C. Keresszegi, D. Ferri, T. Mallat and A. Baiker, *J. Phys. Chem. B*, 2005, **109**, 958–967.
59 D. M. Meier, A. Urakawa and A. Baiker, *J. Phys. Chem. C*, 2009, **113**, 21849–21855.
60 D. Ferri and A. Baiker, *Top. Catal*., 2009, **52**, 1323–1333.
61 B. Veisz, Z. Király, L. Tóth and B. Pécz, *Chem. Mater*., 2002, **14**, 2882–2888.
62 Y. Li, E. Boone and M. A. El-Sayed, *Langmuir*, 2002, **18**, 4921–4925.
63 R. van Hardeveld and F. Hartog, *Surf. Sci*., 1969, **15**, 189–230.
64 G. C. Bond, P. A. Sermon, G. Webb, D. A. Buchanan and P. B. Wells, *J. Chem. Soc., Chem. Commun*., 1973, 444–445.
65 M. Haruta, T. Kobayashi, H. Sano and N. Yamada, *Chem. Lett*., 1987, 405–408.
66 G. J. Hutchings, *J. Catal*., 1985, **96**, 292–295.
67 (*a*) M. Haruta, *Catal. Today*, 1997, **36**, 153–166; (*b*) G. C. Bond and D. T. Thompson, *Catal. Rev. Sci. Eng*., 1999, **41**, 319–388; (*c*) G. C. Bond and D. T. Thompson, *Gold Bull*., 2000, **33**, 41–50; (*d*) M. Haruta, *CATTECH*, 2002, **6**, 102–115; (*e*) M. Haruta, *Chem. Rec*., 2003, **3**, 75–87; (*f*) M. Haruta, *Gold Bull*., 2004, **37**, 27–36; (*g*) A. S. K. Hashmi and G. J. Hutchings, *Angew. Chem., Int. Ed*., 2006, **45**, 7896–7936; (*h*) T. Ishida and M. Haruta, *Angew. Chem., Int. Ed*., 2007, **46**, 7154–7156; (*i*) B. K. Min and C. M. Friend, *Chem. Rev*., 2007, **107**, 2709–2724;

(*j*) S. A. K. Hashmi, *Chem. Rev.*, 2007, **107**, 3180–3211; (*k*) G. J. Hutchings, *Chem. Commun.*, 2008, 1148–1164; (*l*) G.J. Hutchings, M. Brust and H. Schmidbaur, *Chem. Soc. Rev.*, 2008, **37**, 1759–1765; (*m*) A. Corma and H. Garcia, *Chem. Soc. Rev.*, 2008, **37**, 2096–2126; (*n*) G. J. Hutchings, *J. Mater. Chem.*, 2009, **19**, 1222–1235; (*o*) P. Garcia, M. Malacria, C. Aubert, V. Gandon and L. Fensterbank, *ChemCatChem*, 2010, **2**, 493–497.

68 (*a*) A. Abad, P. Concepción, A. Corma and H. García, *Angew. Chem., Int. Ed.*, 2005, **44**, 4066–4069; (*b*) N. Zheng and G. D. Stucky, *Chem. Commun.*, 2007, 3862–3864; (*c*) P. Haider and A. Baiker, *J. Catal.*, 2007, **248**, 175–187; (*d*) F. Z. Su, Y. M. Liu, L. C. Wang, Y. Cao, H. Y. He and K. N. Fan, *Angew. Chem., Int. Ed.*, 2008, **47**, 334–337; (*e*) L. C. Wang, Y. M. Liu, M. Chen, Y. Cao, H. Y. He and K. N. Fan, *J. Phys. Chem. C*, 2008, **112**, 6981–6987; (*f*) T. Mitsudome, A. Noujima, T. Mizugaki, K. Jitsukawa and K. Kaneda, *Adv. Synth. Catal.*, 2009, **351**, 1890–1896; (*g*) T. Ishida, M. Nagaoka, T. Akita and M. Haruta, *Chem.–Eur. J.*, 2008, **14**, 8456–8460; (*h*) H. Miyamura, R. Matsubara, Y. Miyazaki and S. Kobayashi, *Angew. Chem., Int. Ed.*, 2007, **46**, 4151–4154; (*i*) N. Dimitratos, A. Villa, D. Wang, F. Porta, D. S. Su and L. Prati, *J. Catal.*, 2006, **244**, 113–121; (*j*) D. Wang, A. Villa, P. Spontoni, D. S. Su and L. Prati, *Chem.–Eur. J.*, 2010, **16**, 10007–10013; (*k*) L. Wang, X. Meng and F. Xiao, *Chin. J. Catal.*, 2010, **31**, 943–947.

69 H. Tsunoyama, H. Sakurai, Y. Negishi and T. Tsukuda, *J. Am. Chem. Soc.*, 2005, **127**, 9374–9375.

70 H. Tsunoyama, H. Sakurai and T. Tsukuda, *Chem. Phys. Lett.*, 2006, **429**, 528–532.

71 H. Tsunoyama, N. Ichikuni, H. Sakurai and T. Tsukuda, *J. Am. Chem. Soc.*, 2009, **131**, 7086–7093.

72 T. Tsukuda, H. Tsunoyama and H. Sakurai, *Chem.–Asian J.*, 2011, **6**, 736–748.

73 A. Bongiorno and U. Landman, *Phys. Rev. Lett.*, 2005, **95**, 106102.

74 B. N. Zope, D. D. Hibbitts, M. Neurock and R. J. Davis, *Science*, 2010, **330**, 74–78.

75 A. Abad, A. Corma and H. García, *Chem.–Eur. J.*, 2008, **14**, 212–222.

76 P. Haider, B. Kimmerle, F. Krumeich, W. Kleist, J. D. Grunwaldt and A. Baiker, *Catal. Lett.*, 2008, **125**, 169–176.

77 P. Haider, J. D. Grunwaldt and A. Baiker, *Catal. Today*, 2009, **141**, 349–354.

78 Y. Liu, H. Tsunoyama, T. Akita and T. Tsukuda, *J. Phys. Chem. C*, 2009, **113**, 13457–13461.

79 Y. Liu, H. Tsunoyama, T. Akita and T. Tsukuda, *Chem. Lett.*, 2010, **39**, 159–161.

80 M. Hayashi, K. Yamada, S. Nakayama, H. Hayashi and S. Yamazaki, *Green Chem.*, 2000, **2**, 257–260.

81 C. Keresszegi, T. Mallat and A. Baiker, *New J. Chem.*, 2001, **25**, 1163–1167.

82 F. Zaccheria, N. Ravasio and R. Fusi, *Chem. Commun.*, 2005, 253–255.

83 A. Friedrich and S. Schneider, *ChemCatChem*, 2009, **1**, 72–73.

84 J. H. Choi, N. Kim, Y. J. Shin, J. H. Park and J. Park, *Tetrahedron Lett.*, 2004, **45**, 4607–4610.

85 W. H. Kim, I. S. Park and J. Park, *Org. Lett.*, 2006, **8**, 2543–2545.

86 R. Karvembu and R. Priyarega, *React. Kinet. Catal. Lett.*, 2006, **88**, 333–338.

87 T. Mitsudome, Y. Mikami, H. Funai, T. Mizugaki, K. Jitsukawa and K. Kaneda, *Angew. Chem., Int. Ed.*, 2008, **47**, 138–141.

88 T. Mitsudome, Y. Mikami, K. Ebata, T. Mizugaki, K. Jitsukawa and K. Kaneda, *Chem. Commun.*, 2008, 4804–4806.

89 K. Shimizu, K. Sugino, K. Sawabe and A. Satsuma, *Chem.–Eur. J.*, 2009, **15**, 2341–2351.

90 W. Fang, Q. Zhang, J. Chen, W. Deng and Y. Wang, *Chem. Commun.*, 2010, **46**, 1547–1549.

91 J. Chen, Q. Zhang, W. Fang, Y. Wang and H. Wan, *Chin. J. Catal.*, 2010, **31**, 1061–1070.

92 W. Fang, J. Chen, Q. Zhang, W. Deng and Y. Wang, *Chem.–Eur. J.*, 2011, **17**, 1247–1256.

93 S. Meenakshisundaram, E. Nowicka, P. J. Miedziak, G. L. Brett, R. L. Jenkins, N. Dimitratos, S. H. Taylor, D. W. Knight, D. Bethell and G. J. Hutchings, *Faraday Discuss.*, 2010, **145**, 341–356.

94 A. Carlsson, A. Puig-Molina and T. V. W. Janssens, *J. Phys. Chem. B*, 2006, **110**, 5286–5293.

95 M. K. Weldon and C. M. Friend, *Chem. Rev.*, 1996, **96**, 1391–1411.

96 G. Fu, X. Xu, X. Lu and H. Wan, *J. Phys. Chem. B*, 2005, **109**, 6416–6421.

97 G. Fu, X. Xu and H. Wan, *Catal. Today*, 2006, **117**, 133–137.

98 P. Mars and D. W. van Krevelen, *Chem. Eng. Sci.*, 1954, **3**(Suppl), 41–59.

99 K. Chen, S. Xie, A. T. Bell and E. Iglesia, *J. Catal.*, 2001, **198**, 232–242.

100 K. Chen, A. T. Bell and E. Iglesia, *J. Catal.*, 2002, **209**, 35–42.

101 L. Mendelovici and J. H. Lunsford, *J. Catal.*, 1985, **94**, 37–50.

102 R. S. Weber, *J. Catal.*, 1995, **151**, 470–474.

103 Y. Lou, H. Wang, Q. Zhang and Y. Wang, *J. Catal.*, 2007, **247**, 245–255.

104 Z. Zhao, Y. Yusuke, Y. Teng, A. Ueda, K. Nakagawa and T. Kobayashi, *J. Catal.*, 2000, **190**, 215–227.

105 Z. Zhang, Z. Zhao and C. Xu, *Chin. Sci. Bull.*, 2005, **50**, 833–840.

106 Y. Lou, Q. Zhang, H. Wang and Y. Wang, *J. Catal.*, 2007, **250**, 365–368.

107 K. T. Queeney, C. R. Arumainayagam, A. Balaji and C. M. Friend, *Surf. Sci.*, 1998, **418**, L31–L38.

108 Y. Wang, D. An and Q. Zhang, *Sci. China Chem.*, 2010, **53**, 337–350.

109 K. Otsuka and Y. Wang, *Appl. Catal., A*, 2001, **222**, 145–161.

110 K. Tabata, Y. Teng, T. Takemoto, E. Suzuki, M. A. Bañares, M. A. Peña and J. L. G. Fierro, *Catal. Rev. Sci. Eng.*, 2002, **44**, 1–58.

111 A. Arena and A. Parmaliana, *Acc. Chem. Res.*, 2003, **36**, 867–875.

112 Y. Li, S. Chen, Q. Zhang and Y. Wang, *Chem. Lett.*, 2006, **35**, 572–573.

113 T. Kobayashi, K. Nakagawa, K. Tabata and M. Haruta, *J. Chem. Soc., Chem. Commun.*, 1994, 1609–1610.

114 T. Kobayashi, N. Guihaume, J. Miki, N. Kitamura and M. Haruta, *Catal. Today*, 1996, **32**, 171–175.

115 F. Arena, G. Gatti, G. Martra, S. Coluccia, L. Stievano, L. Spadaro, P. Famulari and A. Parmaliana, *J. Catal.*, 2005, **231**, 365–380.

116 Y. Wang, W. Yang, L. Yang, X. Wang and Q. Zhang, *Catal. Today*, 2006, **117**, 156–162.

117 Q. Zhang, Y. Li, D. An and Y. Wang, *Appl. Catal., A*, 2009, **356**, 103–111.

118 J. He, Y. Li, D. An, Q. Zhang and Y. Wang, *J. Nat. Gas Chem.*, 2009, **18**, 288–294.

119 M. H. Groothaert, P. J. Smeets, B. F. Sels, P. A. Jacobs and R. A. Schoonheydt, *J. Am. Chem. Soc.*, 2005, **127**, 1394–1395.

120 N. V. Beznis, B. M. Weckhuysen and J. H. Bitter, *Catal. Lett.*, 2010, **138**, 14–22.

121 J. S. Woertink, P. J. Smeets, M. H. Groothaert, M. A. Vance, B. F. Sels, R. A. Schoonheydt and E. I. Solomon, *Proc. Natl. Acad. Sci. U. S. A.*, 2009, **106**, 18908–18913.

122 Y. Li, D. An, Q. Zhang and Y. Wang, *J. Phys. Chem. C*, 2008, **112**, 13700–13708.

123 D. A. Ruddy, N. L. Ohler, A. T. Bell, T. Don and Tilley, *J. Catal.*, 2006, **238**, 277–285.

124 D. An, Q. Zhang and Y. Wang, *Catal. Today*, 2010, **157**, 143–148.

125 A. R. Silva, K. Wilson, A. C. Wgitwood, J. H. Clark and C. Freire, *Eur. J. Inorg. Chem.*, 2006, 1275–1283.

126 E. D. Guerreiro, O. F. Gorriz, J. B. Rivarola and L. A. Arrúa, *Appl. Catal., A*, 1997, **165**, 259–271.

127 K. I. Hadjiivanov and G. N. Vayssilov, *Adv. Catal.*, 2002, **47**, 307–511.

128 M. D. Amridis, J. E. Rekoske, J. A. Dumesic, D. F. Rudd, N. D. Spencer and C. J. Pereira, *AIChE J.*, 1991, **37**, 87–97.

129 S. Irusta, L. M. Cornaglia, E. E. Miró and E. A. Lombardo, *J. Catal.*, 1995, **156**, 167–170.

130 K. Yoshizawa and Y. Shiota, *J. Am. Chem. Soc.*, 2006, **128**, 9873–9881.

131 M. McCoy, *Chem. Eng. News*, 2001, **79**(43), 19–20.

132 T. A. Nijhuis, M. Makkee, J. A. Moulijn and B. M. Weckhusen, *Ind. Eng. Chem. Res.*, 2006, **45**, 3447–3459.

133 M. G. Clerici, G. Bellussi and U. Romano, *J. Catal.*, 1991, **129**, 159–167.

134 (*a*) T. Hayashi, K. Tanaka and M. Haruta, *J. Catal.*, 1998, **178**, 566–575; (*b*) B. Chowdhury, J. J. Bravo-Suárez, M. Daté, S. Tsubota and M. Haruta, *Angew. Chem., Int. Ed.*, 2006, **45**, 412–415.

135 M. Ojeda and E. Iglesia, *Chem. Commun.*, 2009, 352–354.
136 S. Lee, L. M. Molina, M. J. López, J. A. Alonso, B. Hammer, B. Lee, S. Seifert, R. E. Winans, J. W. Elam, M. J. Pellin and S. Vajda, *Angew. Chem., Int. Ed.*, 2009, **48**, 1467–1471.
137 J. Huang, T. Akita, J. Fays, T. Fujitani, T. Takei and M. Haruta, *Angew. Chem., Int. Ed.*, 2009, **48**, 7862–7866.
138 J. Lu, J. J. Bravo-Suárez, A. Takahashi, M. Haruta and S. T. Oyama, *J. Catal.*, 2005, **232**, 85–95.
139 Y. Lei, F. Mehmood, S. Lee, J. Greeley, B. Lee, S. Seifert, R. E. Winsns, J. W. Elam, R. J. Meyer, P. C. Redfern, D. Teschner, R. Schlögl, M. J. Pellin, L. A. Curtiss and S. Vajda, *Science*, 2010, **328**, 224–228.
140 D. Torres, N. Lopez, F. Illas and R. M. Lambert, *J. Am. Chem. Soc.*, 2005, **127**, 10774–10775.
141 (*a*) R. L. Cropley, F. J. Williams, O. P. H. Vaughan, A. J. Urquhart, M. S. Tikhov and R. M. Lambert, *Surf. Sci.*, 2005, **578**, L85–L88; (*b*) R. L. Cropley, F. J. Williams, A. J. Urquhart, O. P. H. Vaughan, M. S. Tikhov and R. M. Lambert, *J. Am. Chem. Soc.*, 2005, **127**, 6069–6076.
142 D. Torres, N. Lopez, F. Illas and R. M. Lambert, *Angew. Chem., Int. Ed.*, 2007, **46**, 2055–2058.
143 R. M. Lambert, F. J. Williams, R. L. Cropley and A. Palermo, *J. Mol. Catal. A: Chem.*, 2005, **228**, 27–33.
144 J. R. Monnier and G. W. Hartley, *J. Catal.*, 2001, **203**, 253–256.
145 J. Lu, M. Luo, H. Lei, X. Bao and C. Li, *J. Catal.*, 2002, **211**, 552–555.
146 J. Lu, M. Luo and C. Li, *Chin. J. Catal.*, 2004, **25**, 5–9.
147 O. P. H. Vaughan, G. Kyriakou, N. Macleod, M. Tikhov and R. M. Lambert, *J. Catal.*, 2005, **236**, 401–404.
148 H. Chu, L. Yang, Q. Zhang and Y. Wang, *J. Catal.*, 2006, **241**, 225–228.
149 Y. Wang, H. Chu, W. Zhu and Q. Zhang, *Catal. Today*, 2007, **131**, 496–504.
150 W. Zhu, Q. Zhang and Y. Wang, *J. Phys. Chem. C*, 2008, **112**, 7731–7734.
151 W. Su, S. Wang, P. Ying, Z. Feng and C. Li, *J. Catal.*, 2009, **268**, 165–174.
152 I. Onal, D. Düzenli, A. Seubsai, M. Kahn, E. Seker and S. Senkan, *Top. Catal.*, 2010, **53**, 92–99.
153 L. Yang, J. He, Q. Zhang and Y. Wang, *J. Catal.*, 2010, **276**, 76–84.
154 H. H. Voge and C. R. Adams, *Adv. Catal.*, 1967, **17**, 151–221.
155 B. J. Wood, H. Wise and R. S. Yolles, *J. Catal.*, 1969, **15**, 355–362.
156 T. Inui, T. Ueda and M. Suehiro, *J. Catal.*, 1980, **65**, 166–173.
157 J. B. Reitz and E. D. Solomon, *J. Am. Chem. Soc.*, 1998, **120**, 11467–11478.
158 X. Wang, Y. Wang, Q. Tang, Q. Guo, Q. Zhang and H. Wan, *J. Catal.*, 2003, **217**, 457–467.
159 V. Duma and D. Hönicke, *J. Catal.*, 2000, **191**, 93–104.
160 E. Ananieva and A. Reitzmann, *Chem. Eng. Sci.*, 2004, **59**, 5509–5517.
161 X. Wang, Q. Zhang, Q. Guo, Y. Lou, L. Yang and Y. Wang, *Chem. Commun.*, 2004, 1396–1397.
162 X. Wang, Q. Zhang, S. Yang and Y. Wang, *J. Phys. Chem. B*, 2005, **109**, 23500–23508.
163 Q. Zhang, Q. Guo, X. Wang, T. Shishido and Y. Wang, *J. Catal.*, 2006, **239**, 105–116.
164 A. Costine, T. O'Sullivan and B. K. Hodnett, *Catal. Today*, 2006, **112**, 103–106.
165 T. Thömmes, S. Zürcher, A. Wix, A. Reitzmann and B. Kraushaar-Czarnetzki, *Appl. Catal., A*, 2007, **318**, 160–169.
166 B. Moens, H. D. Winne, S. Corthals, H. Poelman, R. De Gryse, V. Meynen, P. Cool, B. F. Sels and P. A. Jacobs, *J. Catal.*, 2007, **247**, 86–100.
167 B. Horváth, M. Hronec and R. Glaum, *Top. Catal.*, 2007, **46**, 129–135.
168 S. Yang, W. Zhu, Q. Zhang and Y. Wang, *J. Catal.*, 2008, **254**, 251–262.
169 B. Horváth and M. Hronec, *Appl. Catal., A*, 2008, **347**, 72–80.
170 Y. Wang, W. Zhu and Q. Zhang, *Chin. J. Catal.*, 2008, **29**, 857–865.
171 T. Thömmes, I. Gräf, A. Reitzmann and B. Kraushaar-Czarnetzki, *Ind. Eng. Chem. Res.*, 2010, **49**, 2624–2637.

